General Disclaimer

One or more of the Following Statements may affect this Document

- This document has been reproduced from the best copy furnished by the organizational source. It is being released in the interest of making available as much information as possible.

- This document may contain data, which exceeds the sheet parameters. It was furnished in this condition by the organizational source and is the best copy available.

- This document may contain tone-on-tone or color graphs, charts and/or pictures, which have been reproduced in black and white.

- This document is paginated as submitted by the original source.

- Portions of this document are not fully legible due to the historical nature of some of the material. However, it is the best reproduction available from the original submission.

BOEING SCIENTIFIC RESEARCH LABORATORIES DOCUMENT NAS 7-489

BOEING SCIENTIFIC RESEARCH LABORATORIES

CONTRACT NAS 7-489

Stress Corrosion Cracking of Titanium Alloys: SCC of Aluminum Alloys, Polarization of Titanium Alloys in HCl and Correlation of Titanium and Aluminum SCC Behavior

T. R. Beck, M. J. Blackburn, M. O. Speidel

Quarterly Progress Report No. 11

Covering work done in the

Period of

October 1, 1968 through March 31, 1969

SOLID STATE PHYSICS LABORATORY MARCH 1969

CONTRACT NAS 7-489

Stress Corrosion Cracking of Titanium Alloys: SCC of Aluminum Alloys, Polarization of Titanium Alloys in HCl and Correlation of Titanium and Aluminum SCC Behavior

Quarterly Progress Report No. 11

Covering work done in the

Period of

October 1, 1968 through March 31, 1969

Prepared by

T.R. Beck, M.J. Blackburn, M.O. Speidel

Solid State Physics Laboratory

Boeing Scientific Research Laboratories

Seattle, Washington 98124

TABLE OF CONTENTS

1. SUMMARY

Continued work on titanium alloys shows basic similarities in all SCC susceptible alloy systems regarding the relation of velocity to potential and the transcrystalline cleavage like fracture path and morphology which is independent of crystal structure. The titanium-manganese system shows a transgranular SCC threshold at 10% Mn compared to 5% Al in the titanium-aluminum system. Investigations on hydrogen embrittlement showed very different fracture path morphology and velocity for hydrogen embrittlement and SCC in titanium-manganese alloys.

Extension of the techniques of steady-state velocity measurement under potentiostatic conditions to aluminum alloys revealed many striking similarities in SCC behavior between titanium and aluminum alloys. Both show a mass transport controlled velocity with small stress dependence (region II) and under selected conditions, a lower velocity, strongly stress dependent (region I). The relationship of velocity to potential, concentration of halide ions, and viscosity of glycerol-water solutions in region II is similar and appears to be consistent with the electrochemical mass-transport-kinetic model previously developed for titanium. Analysis of the stress dependent region I suggests an electrochemical kinetics controlled reaction at the crack tip.

2.0 INTRODUCTION

This report describes part of a study of stress corrosion cracking of titanium alloys initiated in July 1965 (1) and continued under NASA sponsorship beginning July, 1966 (2). This is the eleventh Quarterly Report in the series (3, 4, 5, 6, 7, 8, 9, 10, 11) and covers the six month period of October 1, 1968 through March 31, 1969. A short letter report (12) described work in progress in the period of October 1, through December 31, 1968 but did not present detailed results.

The present report represents the individual and collective contributions of the three authors who have collaborated in the design and interpretation of the experiments. SCC of titanium alloys is by M. J. Blackburn, SCC of aluminum alloys is by M. O. Speidel and the remaining two sections by T. R. Beck.

3.0 TECHNICAL DISCUSSION

3.1 SCC of Titanium Alloys

3.1.1 Metallurgical Variables

Experiments in the past six months reported here are divided into several sections, supplementing work reported in previous Quarterly Reports (4, 7).

Titanium alloys may be classified by their phase structure at room temperature. If we confine such a classification to the major constituents present, four classes of alloys may be recognized as shown in Table 1. This classification is of course an oversimplification as transformation may be produced (e.g. martensite) and other phases formed (e.g. ω-phase, α_2-phase) by suitable heat treatments. However, the classification does provide a suitable framework for the work described below.

Table 1 Alloys Tested to Date in this Investigation

1.	α-phase	Ti(6-10%)Al, Ti-5Al-5Sn-5Zr
2.	(α+β)-phase	Ti-8Al-1Mo-1V, Ti-6Al-4V
	(α-phase predominant or matrix.)	Ti75A
3.	(β+α)-phase (β-phase predominant or matrix.)	Ti-8% Mn, Ti-11.6% and 14% Mo
4.	β-phase	Ti-13Cr-11V-3Al

A. <u>α-phase alloys</u> The alloy Ti-5Al-5Sn-5Zn was selected as suitable for a more accurate investigation of such metallurgical parameters as grain size, prior deformation etc. The SCC susceptibility of this alloy has been measured by Curtis et al (13) who also studied the influence of heat treatment. His tests showed the alloy was susceptible to SCC after all heat treatments, and that low temperature heat treatments which precipitated the $Ti_3(Al,Sn)$ phase produced the most susceptible structure.

To date only two groups of results can be reported, the influence of the stress intensity parameter (K_1) on velocity and the influence of hydrogen content on K_{1C} and K_{ISCC}. The material was tested in the as-received condition which has an undefined heat treatment approximating possibly to mill annealing. This as-received material has a K_{1C} value of 85 Ksi $\sqrt{in}$ tested in the transverse direction. When tested in 0.6 M HCl at -500 mv a K_{1SCC} value of $\approx$25 Ksi $\sqrt{in}$ was measured and the variation of velocity of cracking with K value is shown in Fig. 1 the value varying between 2 - 4 x 10^{-3} cm/sec over the K range 26-75 Ksi $\sqrt{in}$. This variation is similar to that observed in duplex annealed Ti-8Al-1Mo-1V. (Heat treatment and grain size studies in this alloy are planned for the next six months).

A limited number of tests has been performed to study the influence of hydrogen charging on the SCC properties of this alloy. Specimens were charged to hydrogen levels of 180 and 370 ppm, solution treated at 850°C and water quenched. The preliminary results from these tests are shown in Fig. 2. Hydrogen, not unexpectedly, reduces the K_{IC} value, to below

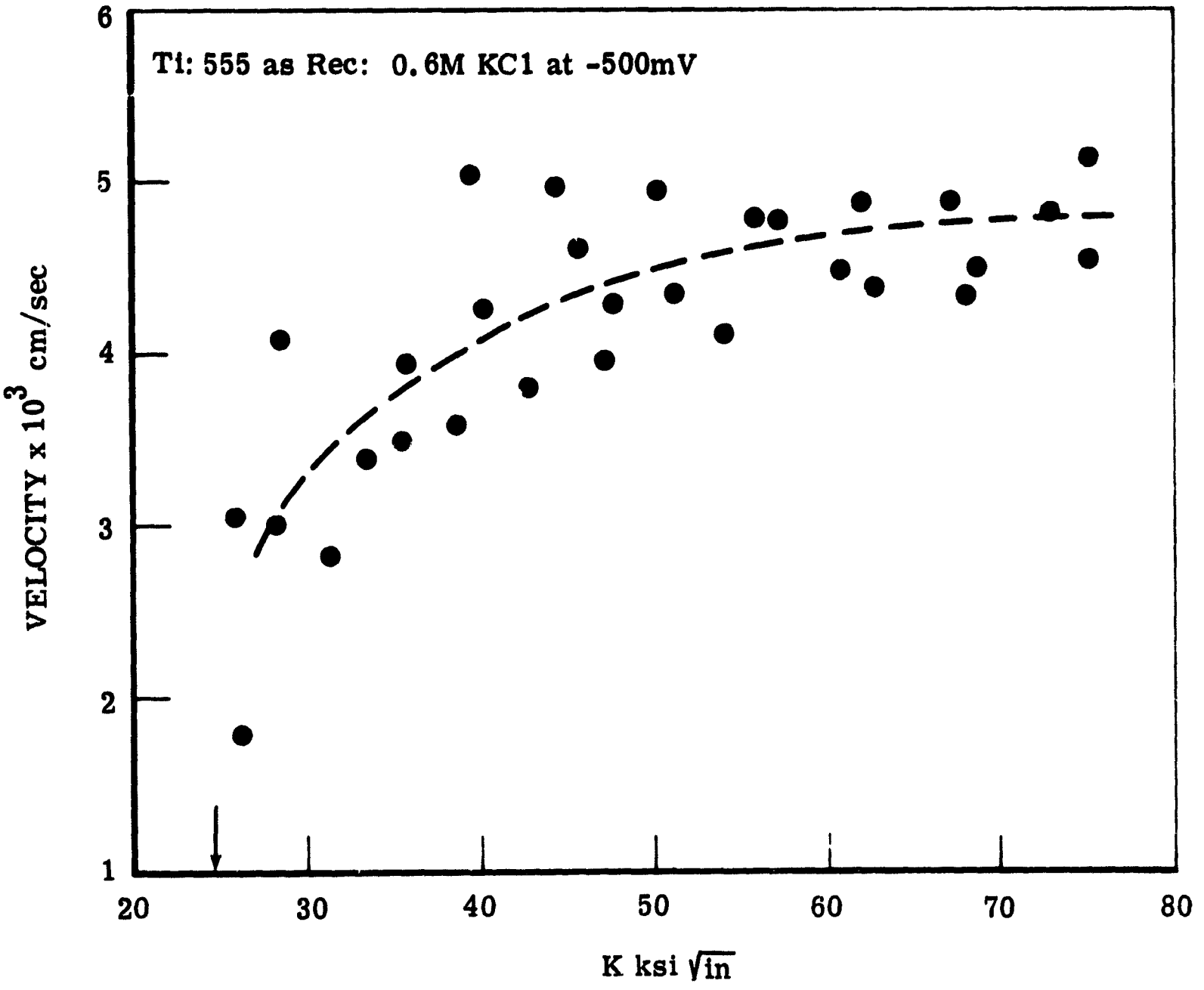

Fig. 1 Variation of fracture toughness of Ti-5Al-5Zr-5Sn with hydrogen content in air and 0.6M KC1 @ -500 mV.

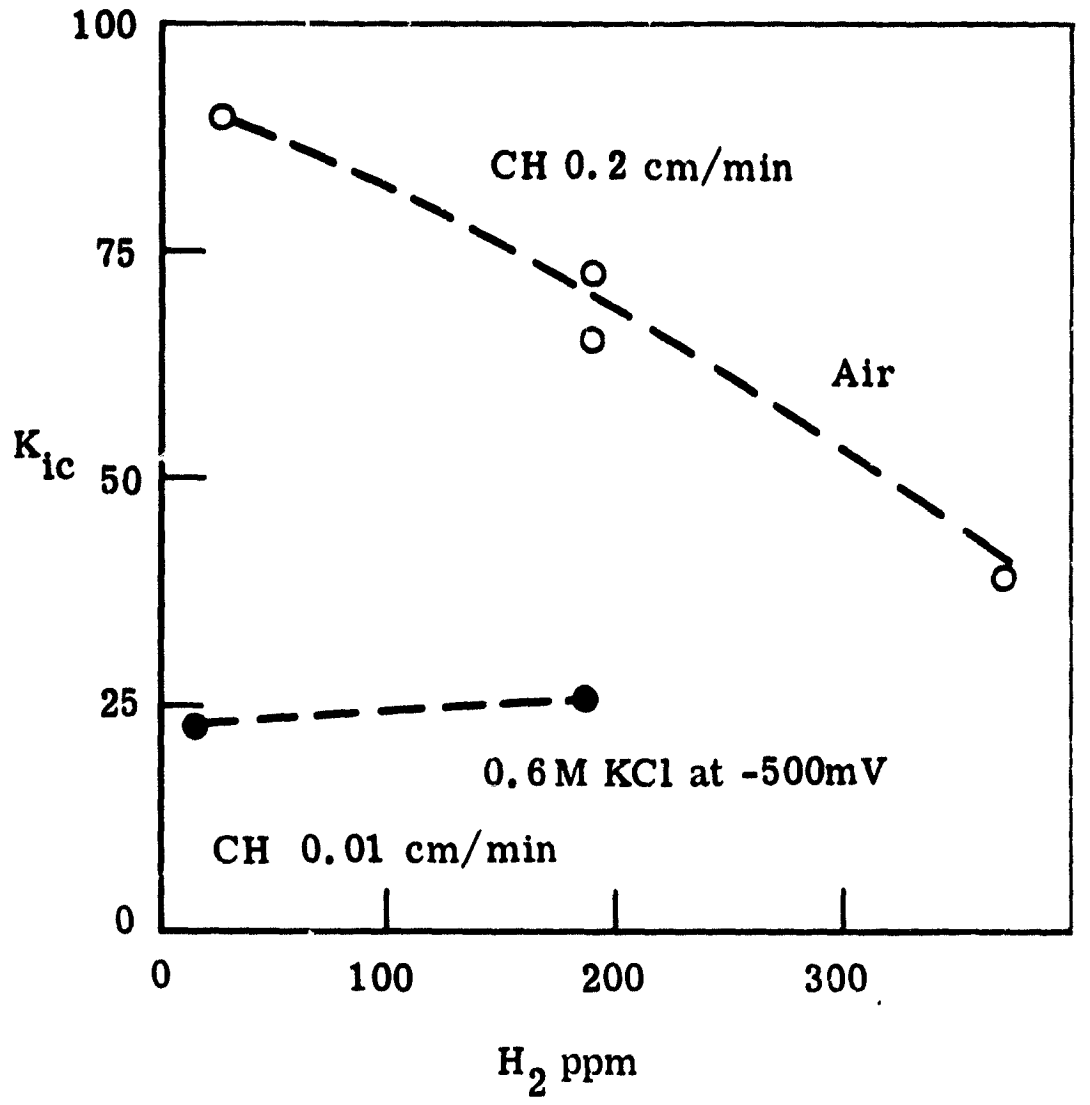

Fig. 2 Velocity of cracking observed in Ti-5Al-5Zr-5Sn tested in 0.6M KCl @ -500 mV.

40 Ksi$\sqrt{in}$ at the 370 ppm level. The fracture mode also changes from a ductile "dimpled" type in the as-received material to an apparent intergranular type in the hydrogen charged material. This is consistent with the observation that additions of aluminum to titanium cause a change in precipitation site of titanium hydride from intergranular sites to the grain boundaries (14). The influence of hydrogen on SCC susceptibility has not been studied in detail, however, at 180 ppm the K_{ISCC} value appears to be little changed from the as-received value (it should be noted that specimens do not have the same heat treatment). However, the velocity of cracking increased from 3×10^{-3} cm/sec to 13×10^{-3} cm/sec in the hydrogen charged material.

B. $\alpha+\beta$ Alloys Work has been concentrated on the Ti-8-1-1 alloy and the results may be divided into two sections. The first is concerned with a new test method and the application of this test in the measurement of slow crack growth rates, i.e., $<10^{-3}$ cm/sec. The second describes the influence of several environmental parameters on crack growth rates.

(a) Double Cantilever Beam (DCB) Specimen

In recent years there has been an increasing tendency to measure fracture properties in terms of the crack extension force (G) or stress intensity parameters (K), such parameters being used to define the fracture toughness of materials. Several types of specimens are used in such tests and in previous reports (1-12) results on SCC cracking have been reported using single edge notched specimens and four point bend specimens. Both specimen configurations result in an increasing K value if the test is

conducted at a fixed deflection (cross head position) and although K can be reduced by cross head movement, unless such movement is performed at a constant rate (and slowly), crack arrest results. The use of double beam cantilever type specimens for fracture toughness testing has been pioneered by Mostovey and Ripling (15) who have defined specimen configuration and the methods of analysis for results. These workers have also applied this type of specimen to SCC testing of steels as have Hyatt (16) and Speidel (17) to SCC testing of aluminum alloys. The obvious advantage of the test is that it enables velocity to be measured as K decreases and also defines K_{1SCC} (at crack arrest).

DCB specimens often require side grooves to maintain the crack in the plane of loading. Fortunately some plate material of Ti-8-1-1 was obtained which did not require side grooving. The specimen dimension used in the tests described below is shown in Fig. 3. The K values calculated from this specimen were computed from crack opening displacement measurements using a formula derived by Hyatt and Smith (18) based on a suggested modification of Mostovoy, Crosley and Ripling (19). The specimens tested were in the as-received condition which appears to approximate to the mill annealed structure.

Variation of crack velocity with stress, or stress intensity for various metallic and nonmetallic systems appears to be divided into three stages which are discussed in more detail in Section 3.4. In previous

notched tensile tests no evidence for crack propagation rates less than 10^{-3} cm/sec has been obtained in aqueous solutions and thus it appeared that no stage I type cracking occurs in Ti alloys. The advantage of the self stressed double cantilever specimen is that K decreases continuously with crack length and thus it is an ideal specimen for investigation of slow crack growth processes.

A series of tests has been conducted in aqueous solution containing various concentrations of Cl^- and at several pH values. The variation of velocity with K in these tests are shown in Fig. 4(a). Tests in 0.6M KCl and/or 1M HCl showed decreasing crack velocities with K until a velocity of $\simeq 10^{-3}$ cm/sec was reached at which velocity level the crack arrested. Specimens were left for times up to 16 hrs after crack arrest which should have enabled growth rates of 10^{-6} - 10^{-7} cm/sec to be detected. It is also of interest that the limiting K value for crack growth (K_{1SCC}) exhibited the dependence on pH observed in notched tensile tests (4). If the tests were conducted in 10M HCl no crack arrest was observed as may be seen in Fig. 4(b) and crack growth rates as low as 10^{-5}cm/sec were measured. Thus in high concentration of Cl^- ions of solution with very low pH values the alloy Ti-8-1-1 shows two regions in crack growth vs K relationships. These two regions are also observed in a saturated solution of KI in methanol. (0.8M), as illustrated in Fig. 5. In this solution the position of the region I curve is shifted by changes in potential as can be seen from the two curves for -500 and +500 mV.

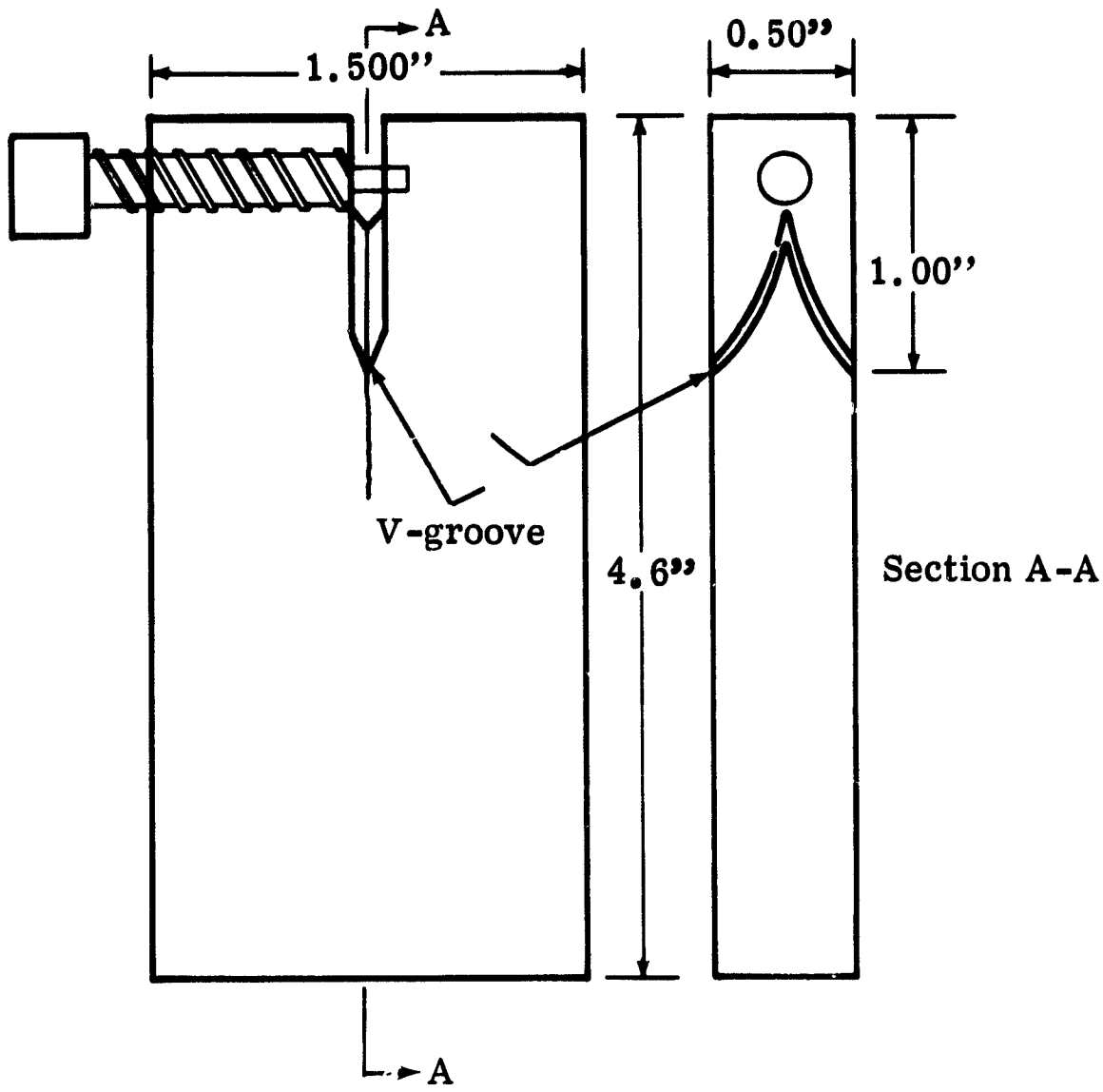

DCB Specimen

Fig. 3 Double beam cantilever (DCB) specimen used in this investigation.

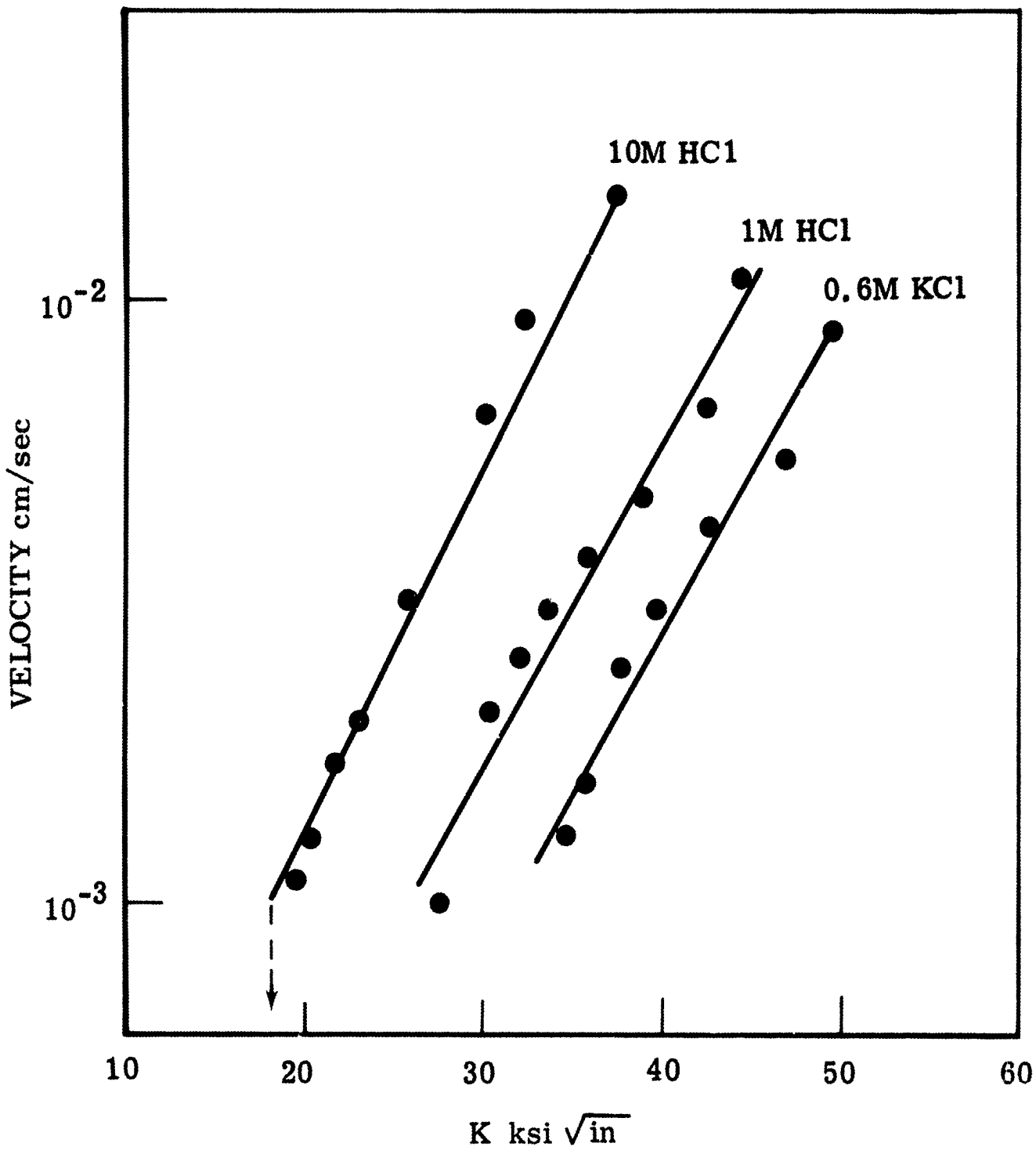

Fig. 4 Variation of crack velocity with stress intensity (K) measured in DCB specimens of Ti:8-1-1 tested in Cl^- solutions.

(a) 0.6M KCl, 1M HCl and 10M HCl

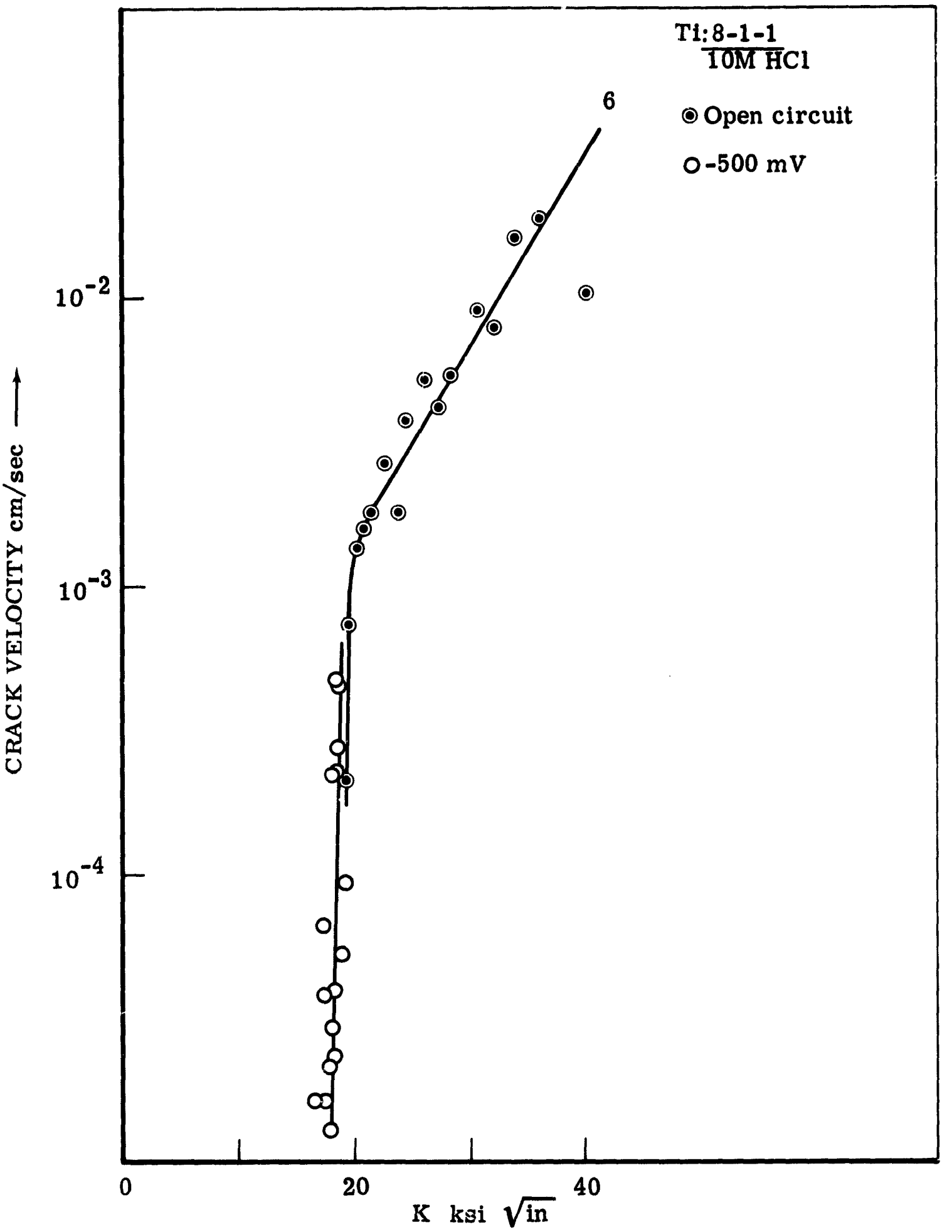

(b) Slow crack growth (Region I) observed in 10M HCl.

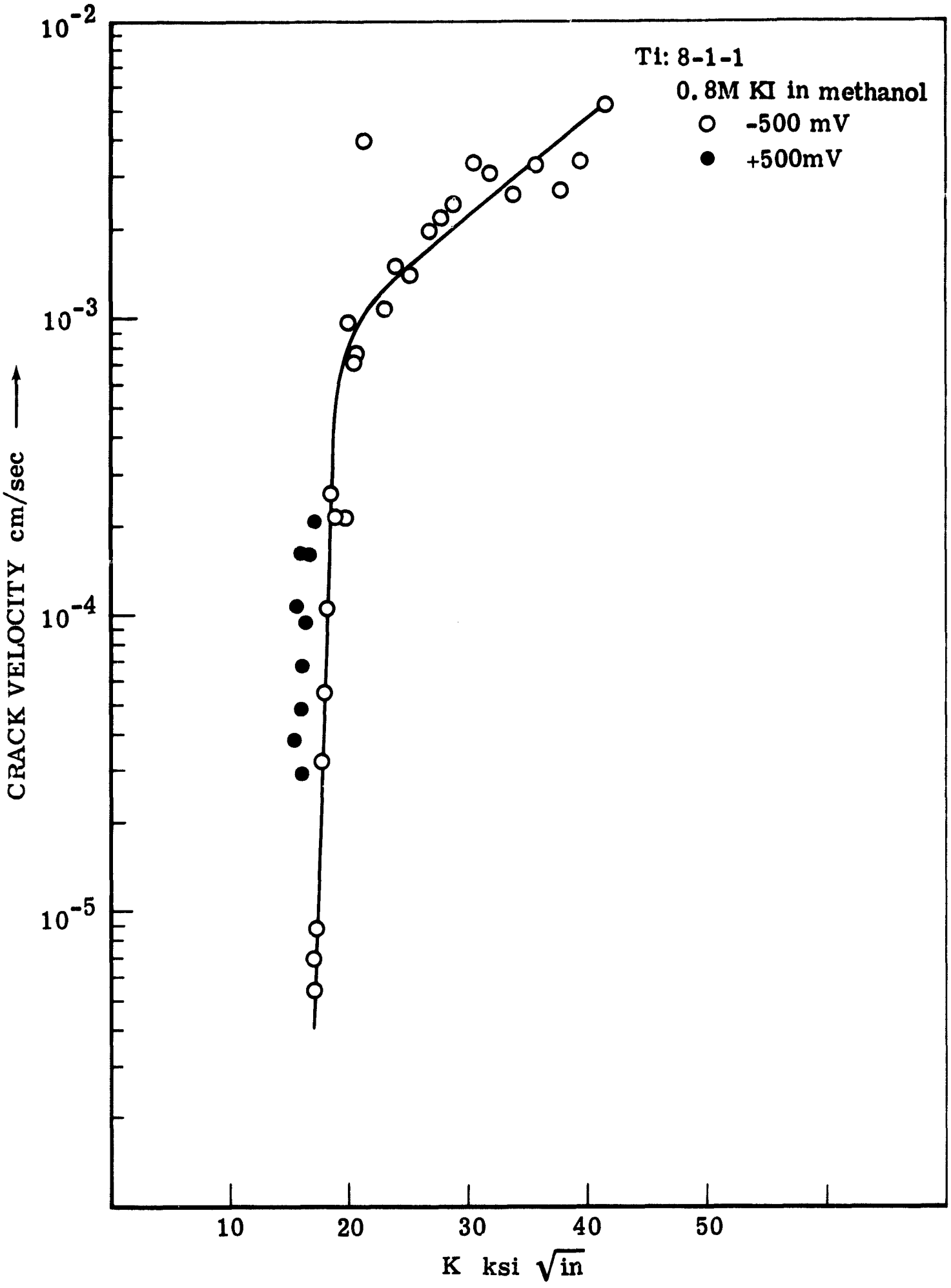

Fig. 5 Slow crack growth (Region I) observed in a 0.8M KI in methanol solution in a DCB specimen of Ti:8-1-1 at -500 and +500 mV.

(b) Environmental Factors

(1) Viscosity: Recent work by Sedricks, et al (20), indicated for pure titanium tested in a series of alcohol-iodine-water mixtures that the time to failure measurements could be correlated with the viscosity of the solutions. From the electrochemical mass-transport-kinetic model for stress corrosion cracking it could be expected that viscosity should be an important parameter controlling the velocity of cracking. A series of experiments has been conducted to study the influence of viscosity on crack growth rates. Initially it was planned to conduct such tests in alcohol with increasing chain length, i.e. the series methyl, ethyl, propyl, butyl, etc., and in glycerol solutions. Approximately 1M solutions of HCl in butyl alcohol and glycerol were prepared by passing dry HCl gas into the solvents. Subsequently a series of 1M HCl glycerol-water solutions was prepared with viscosities ranging from 1-600 cps. The viscosities of these solutions were measured in calibrated falling ball viscometers. Specimens of Ti-8Al-1Mo-1V from sheet 2208 (Mill Annealed) were tested in these solutions. It was found that glycerol had little influence on the initiation load for cracking where-as the 1M HCl butyl alcohol solution required considerably larger loads which is discussed further below. All tests in the HCl-glycerol-water solutions were made under the following controlled loading conditions. Cracking was initiated at a load of 650 Kg and the load held at this value until the crack had propagated for 4 mm. and then the crack propagated under a static cross head condition until the specimen failed. An average

crack velocity over 14 mm. of crack extension was computed from these tests, these results are shown in Fig. 6 and are discussed in Section 3.4.

It was found in the 1M HCl in butyl alcohol solution that a load of 950 Kg was required to initiate cracking and there was no correlation between the velocities measured and those obtained in the HCl-glycerol-water mixtures. Tests in 1M HCl in methanol solution also indicated slower velocities than those obtained in aqueous solution. This may be seen in Table 2 which lists the results obtained in tests in alcohol solutions. The results indicate that parameters other than viscosity control cracking in these solutions and further work is planned to elucidate the SCC properties and the electrochemical properties of titanium alloys in such solutions.

Table 2 SCC Velocities in Water and Alcohol Solutions

Solution	Initial Load Kg	Velocity Cm/Sec.	Viscosity (CPS)
1 M HCl in water	650	40×10^{-3}	1
1 M HCl in methyl alcohol	650	7.18×10^{-3}	0.9
1 M HCl in butyl alcohol	950	1.6×10^{-4} to 1.3×10^{-3}	4.4

(2) The Influence of Ions on Propagating Cracks: In earlier reports it has been shown that only Cl^-, Br^- and I^- ions produce SCC of titanium alloys in aqueous solution. The results on other ions e.g., OH^-, F^-, NO_3^-. SO_4^{2-} etc., showed that crack nucleation did not occur.

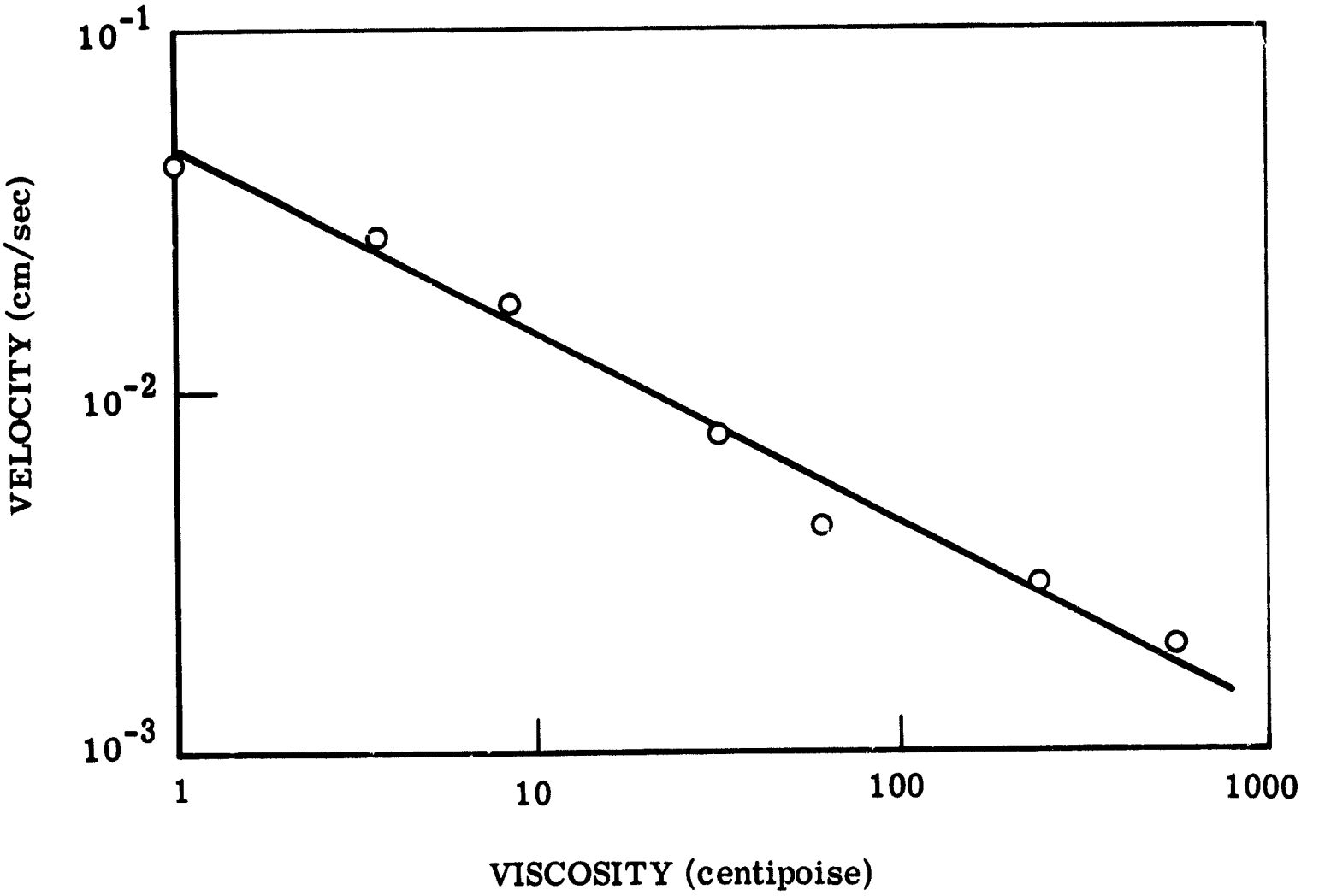

Fig. 6 Variation of crack velocity with viscosity in 1M HCl-water-glycerine solutions.

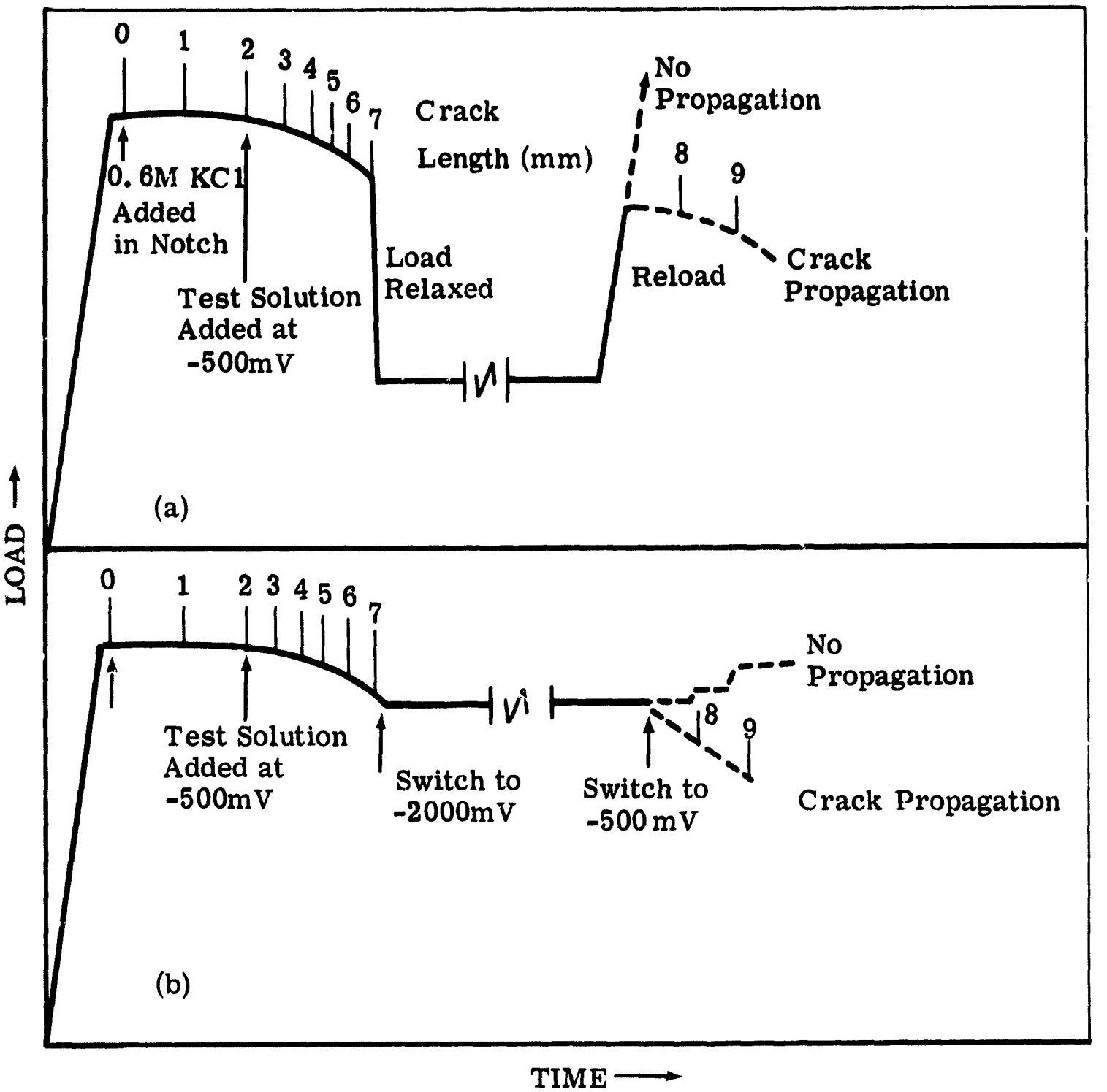

Fig. 7 Diagramatic representation of test procedures used to study influence of various ions on propagating SCC cracks.

A series of experiments has been performed which was designed to study the influence of such ions on the crack propagation stage of SCC. In order to initiate cracking, specimens were loaded to a range in which SCC was known to occur. A drop of 0.6 M KCl was then placed in the notch and after initiation the crack allowed to propagate for 2 mm. The test solution was then introduced into the test cell and the potential controlled at -500 mV, as indicated in Fig. 7 (a&b). The solutions studied were 0.6M NaF, $NaNO_3$, $AgNO_3$, and KOH. In all cases addition of the solution caused the crack to accelerate and the specimen failed unless changes in the conditions were made of the type described below. As cracks continued to propagate in all solutions added either SCC cracks will propagate in virtually any solution, if it has been initiated in Cl^-, or the added solution does not influence or takes a very long time to influence the conditions at the tip of a SCC crack.

To gain further insight into the decay of condition at the crack tip two additional test procedures were examined. In the first type of test, illustrated diagramatically in Fig. 7 (a), the load was relaxed rapidly during crack propagation to a load level at which cracking stopped and held at this load level for various times. The load was then reapplied until SCC cracking reinitiated or the specimen failed mechanically. In all cases the crack reinitiated at the same or slightly lower loads than that before relaxation, no instances of SCC immunity being found. The maximum holding time was 16.5 hours. In the second type of test, illustrated in Fig. 7(b), crack arrest was accomplished by cathodic protection, the potential of the specimen being switched to -2000 mV, and the specimen held

at this potential for various times. The potential was then switched back to -500 mV and the crack then either repropagated or did not. It was found that the repropagation of the crack depended upon the time of holding at -2000 mV and to some extent on the added solution. Thus in 0.6M KOH the minimum time to inhibit crack propagation was 10 mins. and in 0.6M NaF and $NaNO_3$ times of 20-30 mins. were required.

(c) Cathodic Protection It has been reported by Scully (22) that it is not possible to cathodically protect titanium alloys in acidic solutions i.e. HCl etc. In order to define more precisely the limits of cathodic protecti tests have been performed in HCl solution of various concentrations on the alloy Ti-8Al-1Mo-1V in the duplex and mill annealed conditions. The results of these tests are listed in Table 3 . It can be seen that in order for cathodic protection to occur, concentration of the HCl solution must be below 0.3M corresponding to a pH of $\sim$0.5.

A second series of tests was performed to establish if in neutral solution there was an upper limit to the velocity of cracks which could not be arrested by cathodic potential. Specimens from sheet 2279 heat treated to produce a very susceptible structure were tested in the extreme electrochemical condition of saturated KI at a potential of +1000 mV. Under these conditions crack velocities $>10^{-1}$ cm/sec could be produced. It was found that cracks propagating at a velocity of 10^{-1} cm/sec could be arrested at a potential of -2000mV. However cracks propagating at velocities of 1.5×10^{-1} cm/sec were not arrested at a potential of -2000mV although the crack velocity appeared to be reduced at this potential.

Table 3 Limits of HCl Concentration for Cathodic Protection of Ti:8Al-1Mo-1V; Cracks Initiated at -500 mV

Sheet No.	Solution	Maximum Cathodic Potential	Results
2208(mill annealed)	12M HCl	-3000mV	No arrest
	3M HCL	-16,000mV	No arrest
	1M HCl	-10,000mV	No arrest but indication of slower velocity
	0.6M HCl	-6,000mV	No arrest but crack slowed from $25x10^{-3}$cm/sec to $8x10^{-3}$ cm/sec.
	0.3M HCl	-2000mV	No arrest but slower velocity
	0.1M HCl	-2000mV	Crack arrested.
2283(Duplex annealed)	3M HCL	-3000mV	No arrest but crack slowed from $33x10^{-3}$ cm/sec to $11x10^{-3}$ cm/sec.
	1M HCl	-3000mV	No arrest but crack slowed from $5x10^{3}$ to $1.1x10^{-3}$cm/sec.
	0.5M HCl	-3000mV	No arrest but crack slowed from $3.3x10^{-3}$cm/sec to $0.8x10^{-3}$cm/sec.
	0.1M HCl (adjusted to 0.5M Cl^- with Sat KCl)	-3000mV	Crack arrested

C. $\beta+\alpha$ Alloys In quarterly report no. 5 (7) the general features of the SCC susceptibility of the Ti:8%Mn alloy was described. It was shown that the alloy was susceptible to SCC when in the $\alpha+\beta$ condition and two additional experiments have been performed which relate to the compositional factors influencing susceptibility. Further, the result of hydrogen charging, and temperature on the susceptibility of the alloy have been investigated. These results are described in the following sections:

(a) Heat Treatment at 560°C

The eutectoid temperature in the Ti-Mn system is 550°C and thus the specimen heat treated slightly above this temperature consists of a mixture of the α and β phases in the approximate proportions $\alpha:\beta \simeq 2:1$. The α-phase is essentially the matrix phase and the β-phase exists as isolated grains. Testing after this heat treatment has shown that a halide environment has very little influence on the fracture load and no slow growth was observed. The failure load in both air and environment was 3,5000 Kg which should be compared with the results in Fig. 5 of reference (7).

(b) In Ref. (7) it was stated that it was impossible to decide if the criterion for susceptibility of the Ti:8% Mn alloy was the presence of the β-phase or the composition i.e. Mn content, of the β-phase. In order to resolve this question a Ti:16% Mn alloy was obtained and tested; specimens were water quenched from 850°C, which retains the β-phase, and tests

performed in air and in 0.6M KCl at -500 mV. The results for initiation stress and crack velocity are shown in Table 4 which also includes for comparison the data for the Ti:8% Mn alloy heat treated at 700°C (This treatment results in a β-phase with a composition of 12% Mn). It can be seen that the initiation stress is lower and the velocity faster than the corresponding values for the Ti:8% Mn alloy, indicating that it is the composition of the β-phase that controls the SCC susceptibility of Ti-Mn alloys. The fractographic features of the failure surfaces in the 16% Mn alloy fractured in air and solution are shown in Fig. 8(a & b). The alloy shows the usual change from a ductile "dimpled" surface in the air fracture to the flat, almost featureless in this case, cleavage-like appearance of the fracture in Cl^- solution.

(c) Hydrogen Embrittlement

The Ti:8% Mn is an example of an α+β alloy susceptible to slow strain rate hydrogen embrittlement (H.E.). Williams (23) has summarized known features of this phenomenon and Fig. 9 (a & b) taken from this paper summarize the influence of hydrogen content and strain rate on susceptibility to H.E.. In an earlier paper Jaffee and Williams (24) reported on the compositional aspects of susceptibility - classifying alloys on the basis of the minimum hydrogen (H_{min}) content necessary to produce H.E. These results are summarized in Table 5.

(a) Tested in air

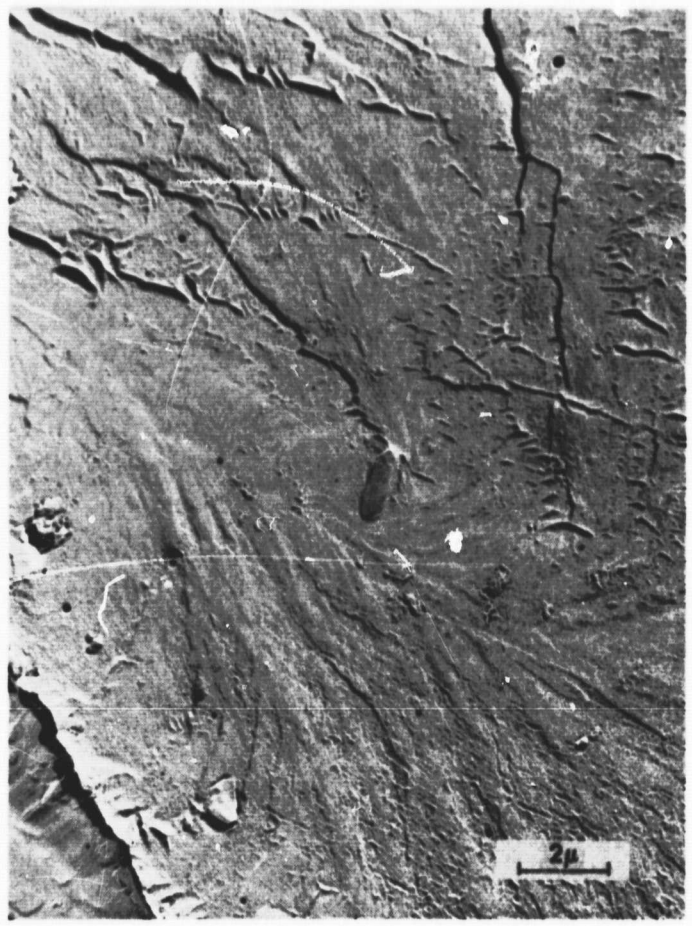

(b) Tested in 0.6M KCl @ -500 mV

Fig. 8 Fracture surfaces observed in Ti:16% Mn alloy, solution treated and quenched from 850°C.

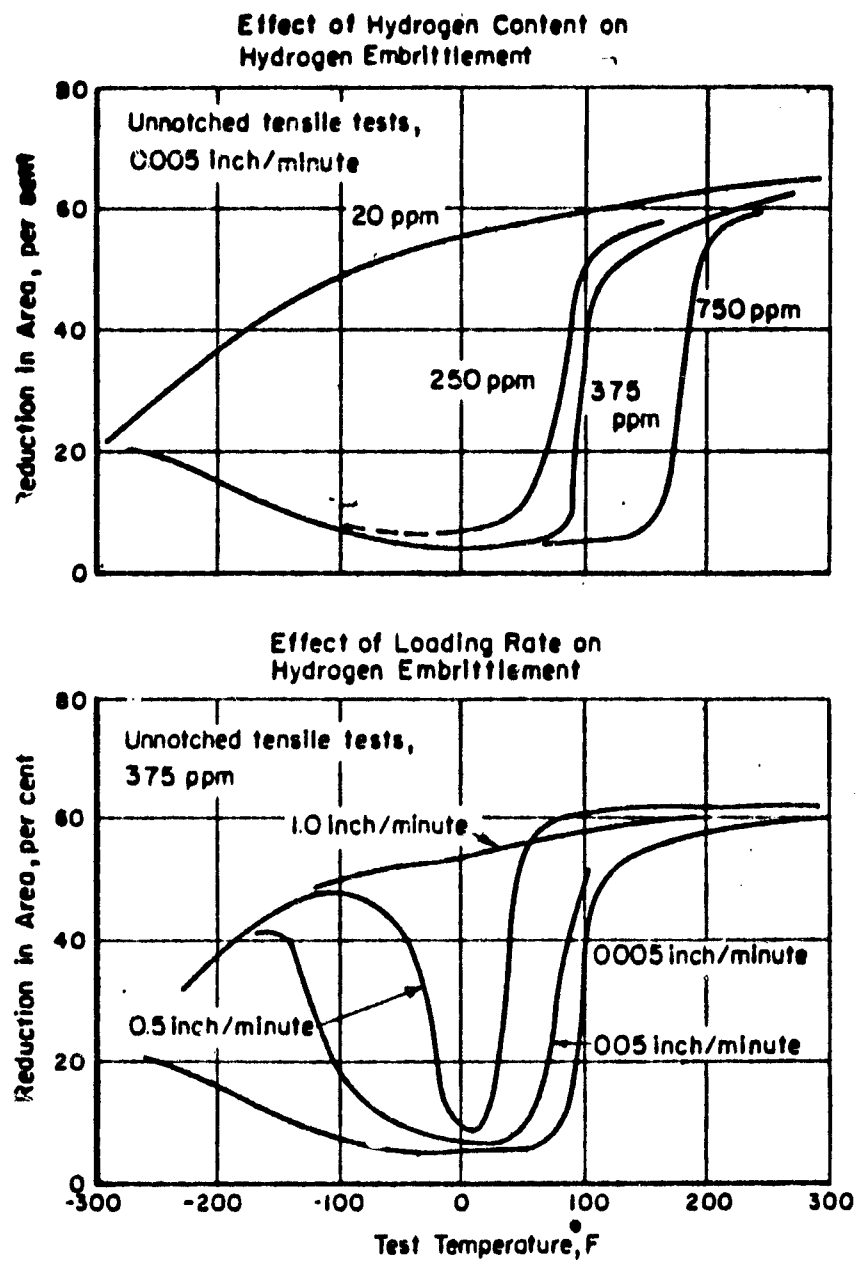

Fig. 9 Effect of hydrogen content, strain rate and temperature on the tensile ductility of a typical ($\alpha+\beta$) titanium alloy (from Ref. 24).

Table 4 Initiation Stress and SCC Velocity in 8% and 16% Manganese Alloy

Alloy		Ti:8% Mn	Ti:16% Mn
Heat Treatment		700°C 160 Hrs.	850°C WQ
Yield Stress		90 Ksi	130 Ksi
Fracture Stress (net area)	Air	161 Ksi	124 Ksi
	Solution*	38 Ksi	28 Ksi
Crack Velocity*		1.2×10^{-2} cm/sec	4.0×10^{-2} cm/sec

*0.6M KCl @ -500 mV

Table 5 Summary of Hydrogen Embrittlement Data of Williams and Jaffee (24)

Ti:Mo - no influence of H above 4% Mo. In the 4% Mo alloy H_{min} =800 ppm.

Ti:Mc:Al(4-6%) - eliminated susceptibility of 4% Mo alloy

Ti:Mo:Sn(12%) - eliminated susceptibility of 4% Mo alloy

Ti:V. The H_{min} content increases from 20 ppm (4%V) to 800 ppm (20%V)

Ti:4V:6Al - Aluminum increased H_{min} to 400-600 ppm

Ti:Mn - The H_{min} content increased from 20-200 ppm (4% Mn) to 300-400 ppm (8% Mn)

Ti:4Mn:4Al - Aluminum increased H_{min} to 200-300 ppm

Ti:6Al - Aluminum increased H_{min} 800 ppm

Ti:4%Fe - H_{min} 200 ppm

Ti:4Fe:6Al - Al increased H_{min} to 400-600 ppm

Ti:Cr - H_{min} increased from 20-200 ppm (4%Cr) to 400-600 ppm (8% Cr).

In most of the above systems increased oxygen content lowered the H_{min} value. It appears that there is some correlation between the systems susceptible to SCC and those susceptible to HE. However, from the above list two differences can be detected, firstly the H_{min} values tend to fall with increasing solute content, and secondly aluminum tends to increase H_{min} values in all cases. The opposite trend is observed in SCC susceptibility, Ti:16Mn is more susceptible than Ti:8Mn and in the Ti:6Al:4V alloy it is the aluminum which is considered responsible for SCC susceptibility.

In order to study further any similarity or differences between SCC and HE the influence of hydrogen charging on the properties of the Ti:8% Mn alloy has been studied. Specimens were aged at 650°C for 1 week to develop a coarse $\alpha+\beta$ structure and were then charged with 500($\pm$20) ppm of hydrogen in a Sieverts Apparatus. The charged specimens were tested in silicone oil, at slow and fast strain rates, and in 0.6M HCl @ -500°C. Tests were conducted at 23 and 90°C. In the H.E. study, specimens were step loaded in 100 Kg increments and sufficient time elapsed between each loading step to detect crack growth rates of $<5x10^{-5}$ cm/sec. Fig. 10 lists the velocity results obtained for crack propagation in an SCC and HE condition and also includes the net area fracture stresses for crack initiation in the HE and SCC tests and the fracture stresses in fast strain rate tests. It can be seen that increasing the temperature increases the initiation stress for HE as would be expected from Fig. 9. The velocity of cracking also increases but this could be due to the rather large stress difference. The equivalent tests in 0.6M KCl show that the cracking rate is 2 orders of magnitude faster and if the tests at 23°C were conducted at the same stress level this difference increased to 3 orders of magnitude. The

crack velocities for hydrogen charged specimen were slightly higher than uncharged specimens and tested under SCC conditions, and it should also be noted that the initiation stress is somewhat lower for the charged specimen.

The features of the crack path and surface were analyzed by optical microscopy and replica electron microscopy techniques. Fig. 11(a and b) illustrates that the crack path of a crack propagated under H.E. conditions is predominantly intergranular, this is probably due to the continuous film of the α-phase present at the grain boundaries. Under SCC conditions the crack path is predominantly transgranular as may be seen from Fig. 12 (a and b). Analysis of the fracture surface generated by H.E. show two types of fracture features: planar areas as shown in Fig. 13 which may represent areas of intergranular separation, and other regions shown in Fig. 14 which contain rather ill defined "dimples" some of which contain lamella particles, e.g. at A, which may be α-phase plates. The fracture surface produced under SCC conditions shows the typical cleavage like markings as shown in Fig. 15 . To illustrate more clearly the differences in fracture appearance between H.E. and SCC cracks, a crack was extended under H.E. conditions and then 0.6M KCl added to the cracked region which caused very rapid crack extention. Fig. 16 shows the interface between the H.E. and SCC crack. For completeness Fig. 17 shows the fracture surface features of a specimen broken at a high strain rate which shows a "dimpled" fracture topology similar in some ways to Fig. 14.

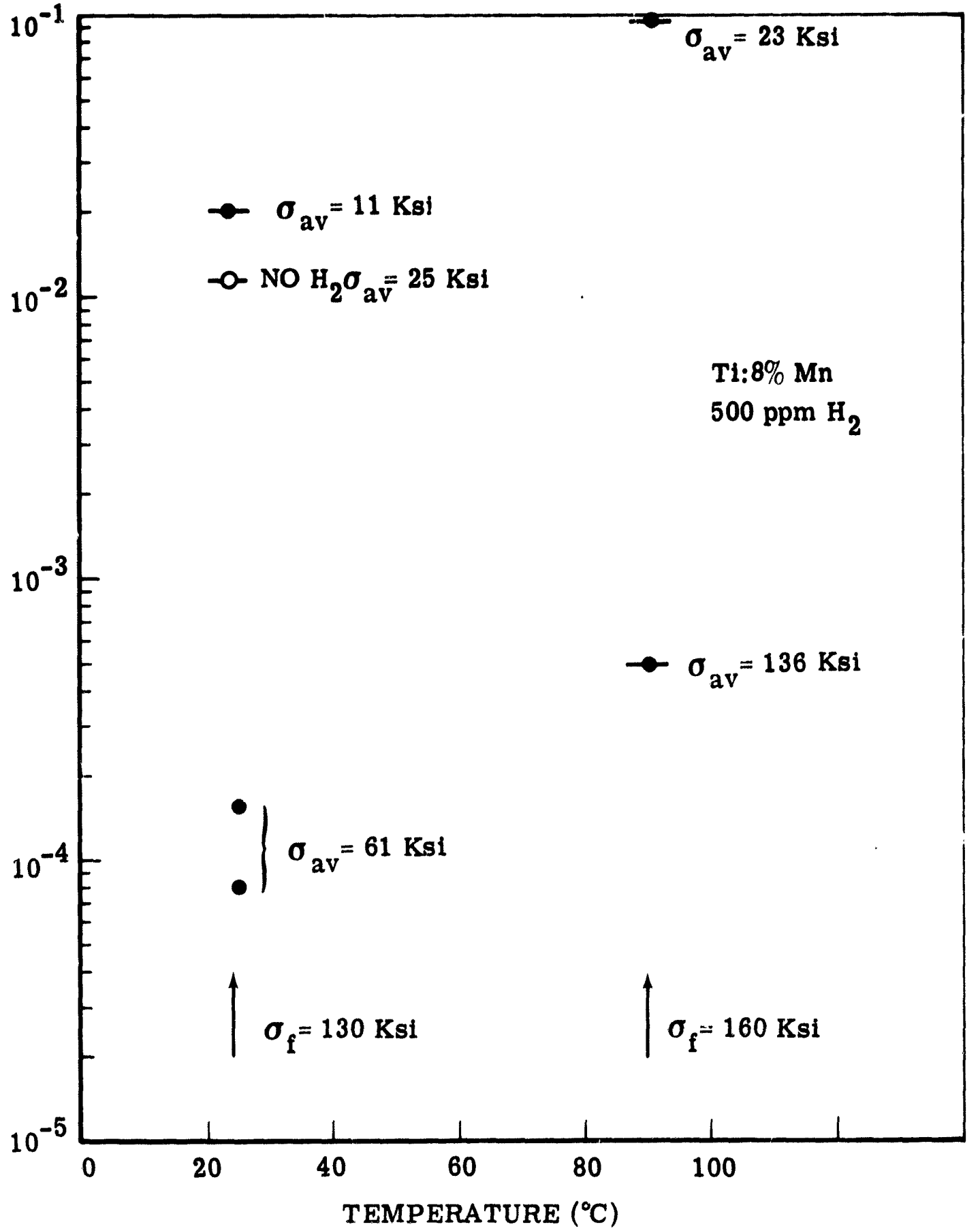

Fig. 10 The influence of hydrogen content and environment on crack velocity and nucleation stress in the Ti8% Mn alloy (heat treated for 1 week @ 650°C). σ_{av} = nucleation net area stress: σ_f = fracture stress in air at a high strain rate.

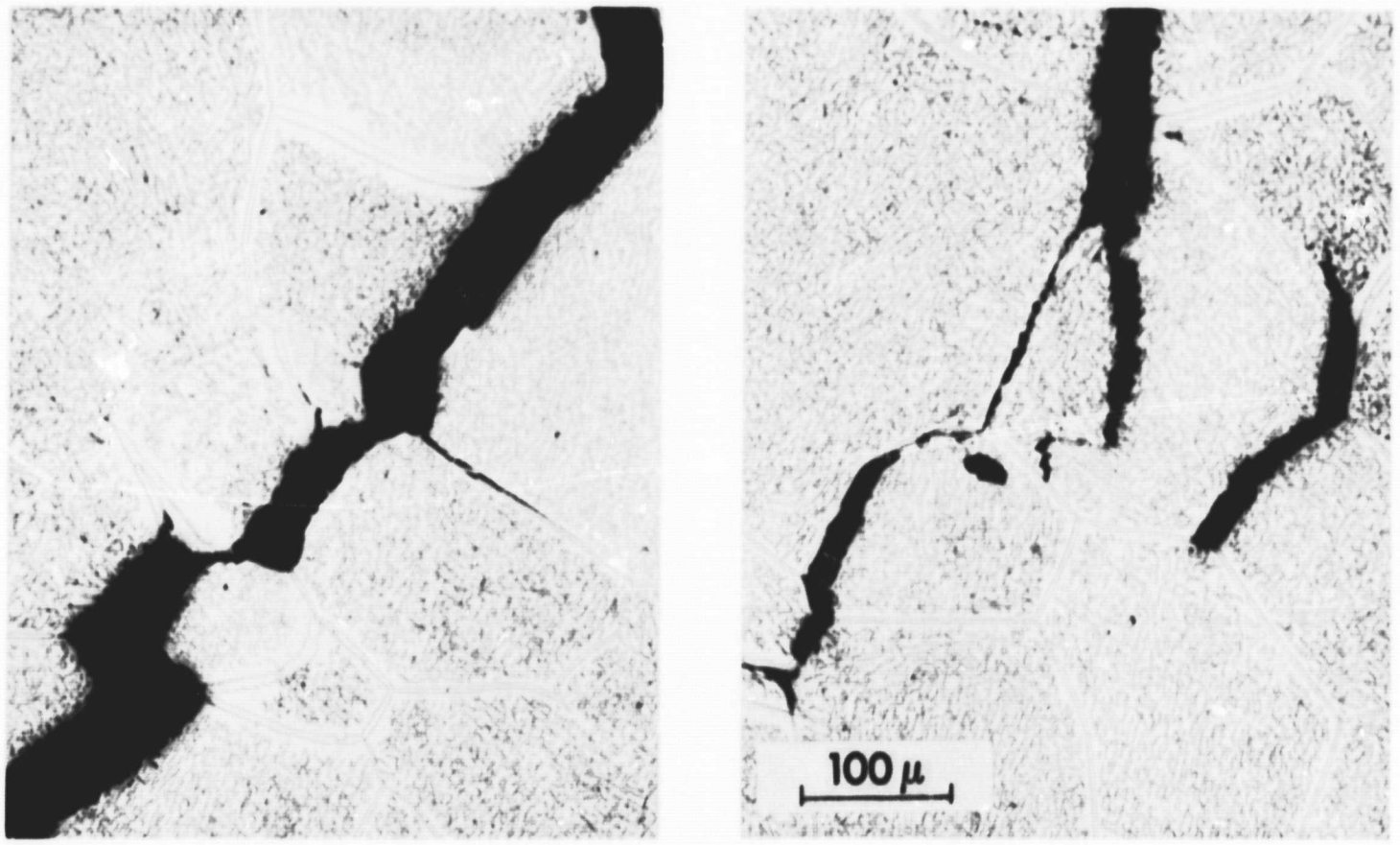

Fig. 11(a&b) Optical micrographs of fracture path for a crack propagated under hydrogen embrittlement conditions in Ti:8% Mn(500 ppmH)

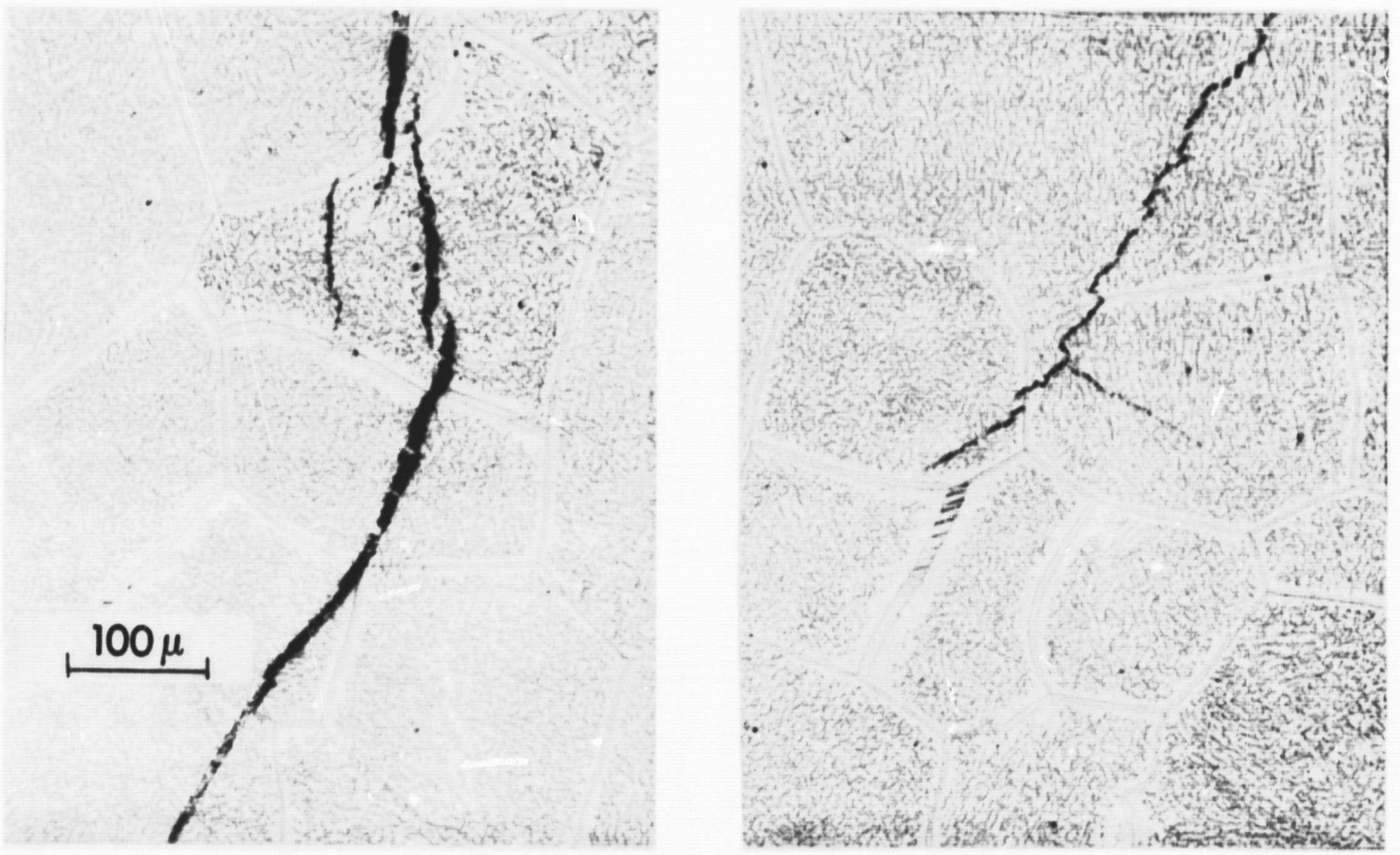

Fig. 12(a&b) Optical micrographs of fracture path under SCC conditions in Ti 8% Mn (500 ppm H).

Fig. 13 Fracture surface of Ti 8% Mn (500 ppm H) failed by hydrogen embrittlement - note flat faceted surface.

Fig. 14 as 13 - Note irregular dimpled region and possible α-particles at A.

Fig. 15 Fracture surface of Ti 8% Mn (500 ppm H) failed under SCC conditions - Note cleavage like appearance.

Fig. 16 Interface between hydrogen embrittlement and SCC fracture regions observed in Ti 8% Mn (500 ppm H).

Fig. 17 Fracture surface observed in a Ti 8% Mn failed in air at a fast strain rate.

D. β-phase Alloys The alloy Ti:13V-11Cr-3Al (VCA120) was selected to study the SCC properties of an all β-phase alloy. In this alloy the β-phase can be retained on quenching from above the transus temperature which is ≈720°C. The β-phase is metastable and will decompose on ageing at temperatures below 720°C:

$$\beta \rightarrow \beta + \alpha \rightarrow \beta+\alpha+TiCr_2$$

However, as at this time the alloy has only been tested in the all β-condition, it is not necessary to consider the nature of these trans-formations. It has been shown that this alloy is susceptible to SCC in aqueous salt solutions (25) but it was considered worthwhile to define this susceptibility in more detail.

Standard single-edge notched specimens were quenched from various temperatures above the β-transus and tested in 0.6M Cl^- and I^- solutions at various potentials. The variation of initiation load with potential for several solution treatment temperatures is shown in Fig. 18 which shows that the minimum values occur at -500 mV and that the general shape of the curve is the same as that found for α, α+β and β+α alloys. The only difference observed is that initiation loads in I^- solution at +500 mV are slightly higher than those observed at -500 mV. Differences in the initiation loads observed after the various solution treatment temperatures are attributed at this time to differences in grain size which is discussed in more detail below. If the velocity of cracking measured in these tests

were plotted against potential it was found that a general upward trend of velocity was observed, however, that the scatter was considerably greater than those observed in $\alpha+\beta$ or $\beta+\alpha$ alloys. Two factors in addition to potential have been found to exert a strong influence on crack velocity, these are grain size and stress. Fig.19 shows the variation of crack velocity with grain size and initial load, measured in static cross head tests at a potential of -500 mV. If these curves are used to correct for the influence of initial load on velocity, and assuming that the relationships are independent of potential, the velocity variation with potential may be obtained. This relationship is shown in Fig.20 from which it can be seen that velocity varies linearly with potential as found in $\alpha+\beta$ and $\beta+\alpha$ alloys.

The influence of grain size on initiation stress has been studied in 0.6M KCl at -500 mV. Grain size was varied by producing various reductions in thickness by cold rolling and subsequently annealing at temperatures above the β-transus for controlled times. Specimen thickness varied in these tests and if the state of stress is an important variable the values obtained may not reflect the influence of grain size alone. The variation of the net area stress to initiate cracking with the reciprocal of the grain diameter (d) is shown in Fig. 21. It is evident that the stress to initiate cracking increases with decreasing grain size, however the dependence appears nearer to $(1/d)$ rather than $(1/d)^{\frac{1}{2}}$. The latter (Hall-Petch) relationship has been observed in some SCC systems (26), usually in time to failure measurements.

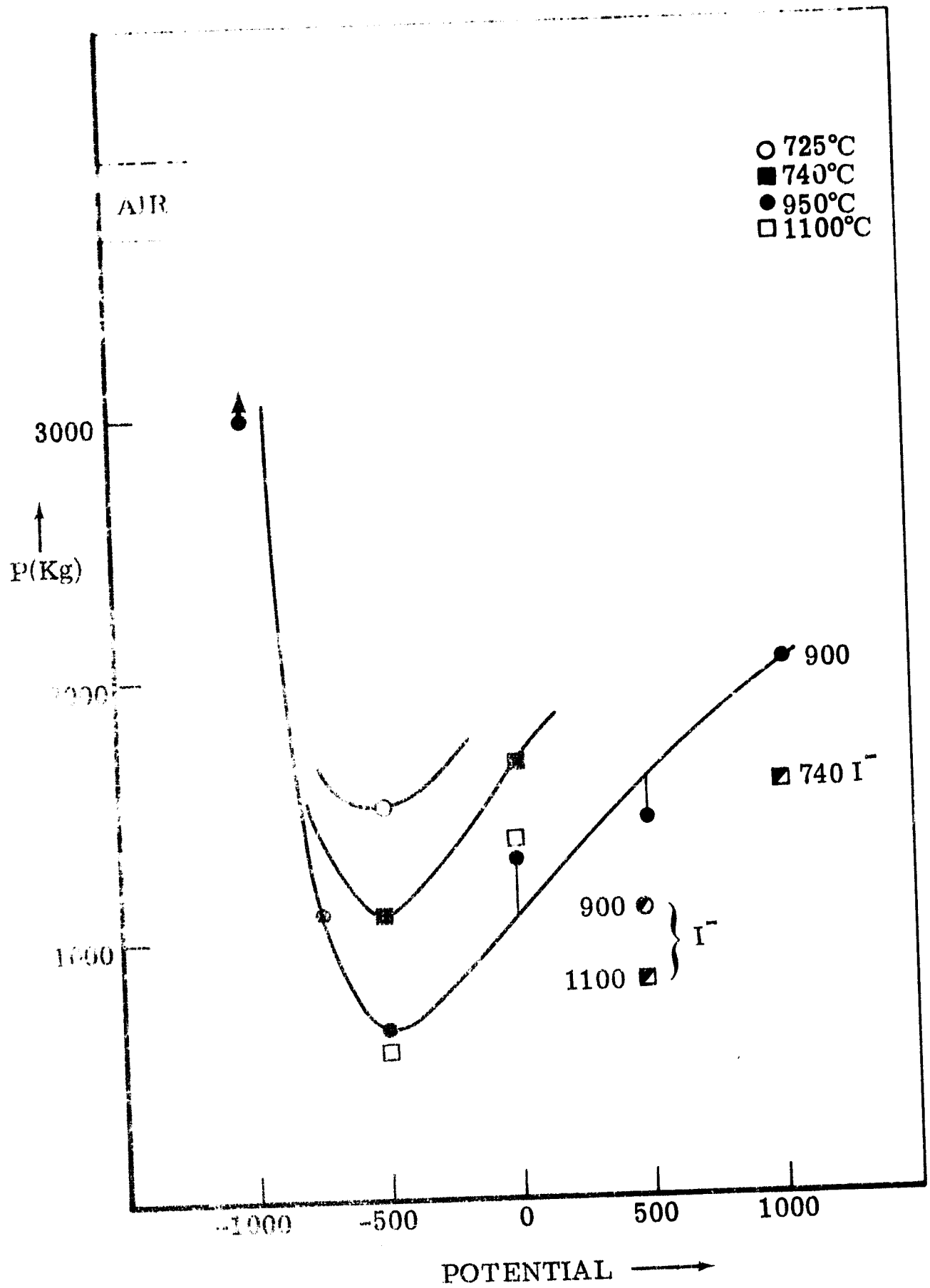

Fig. 18 Variation of fracture load with potential and solution treatment temperature in Ti:13V:11Cr:3Al tested in 0.6M KCl and KI at several potentials.

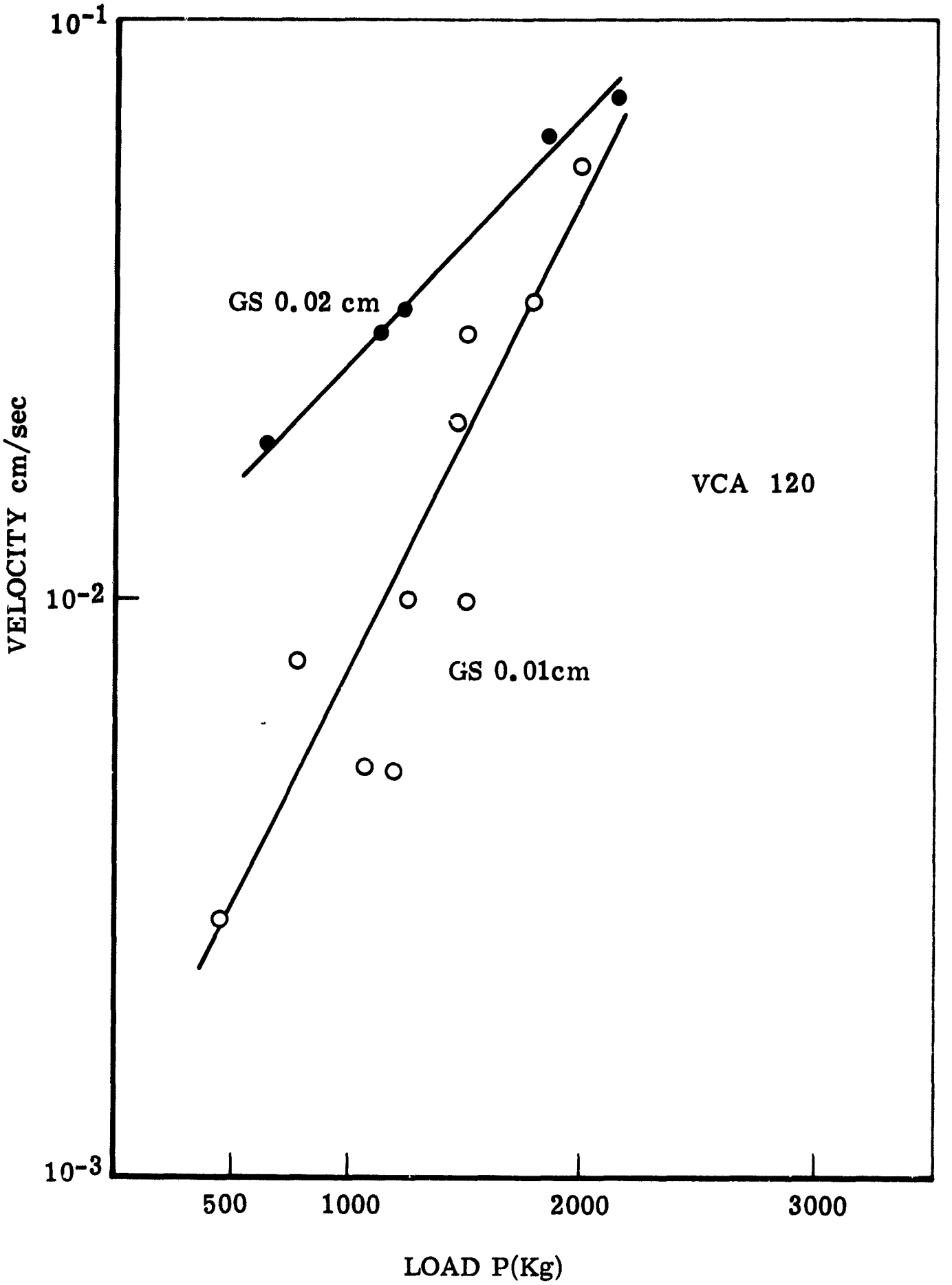

Fig. 19 Variation of velocity of cracking with grain size and initial load in Ti:13V:11Cr:3Al tested in 0.6M KCl at -500 mV.

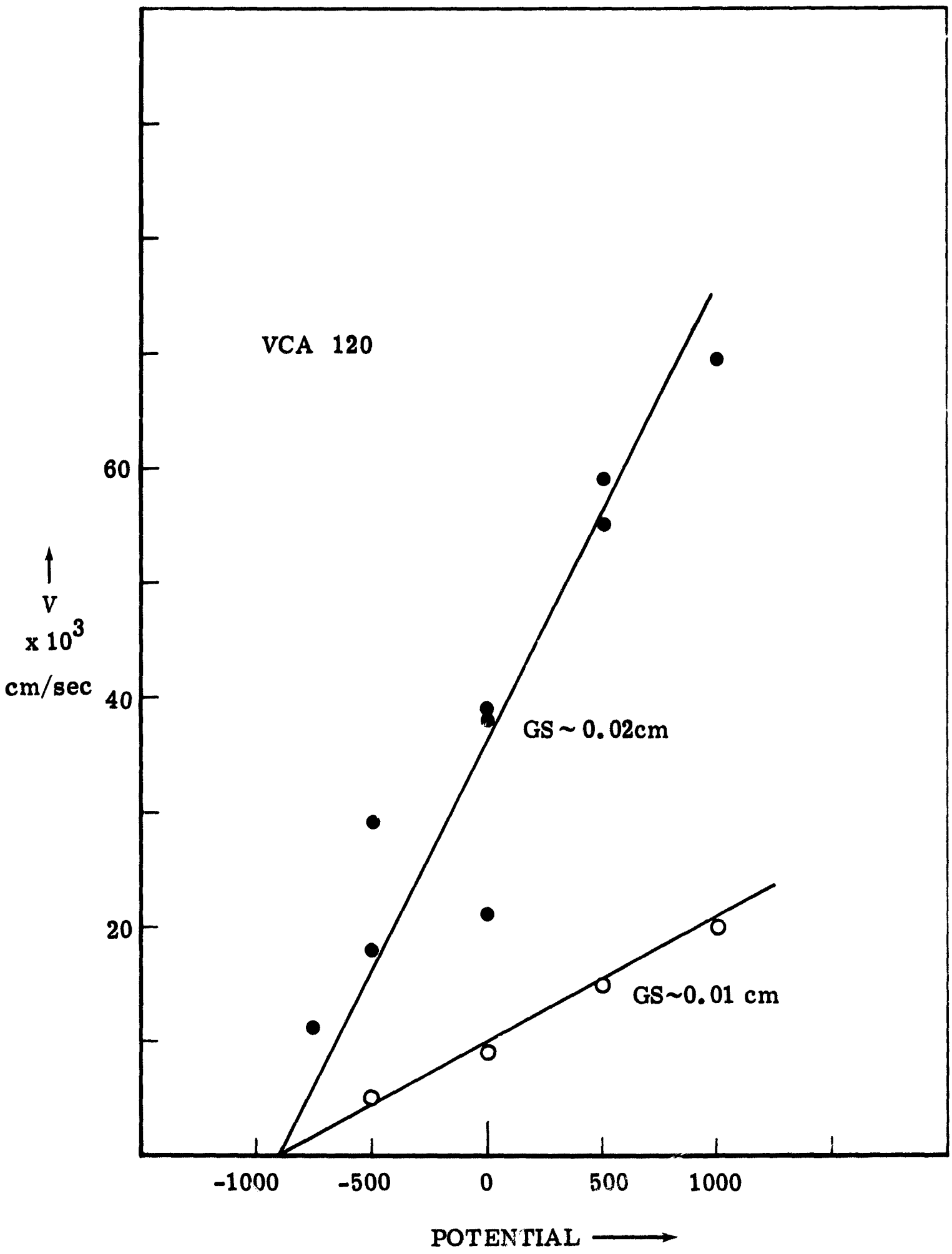

Fig. 20 Variation of velocity with potential and grain size in Ti:13V:11Cr:3Al after correcting for intial load values (see Fig. 19).

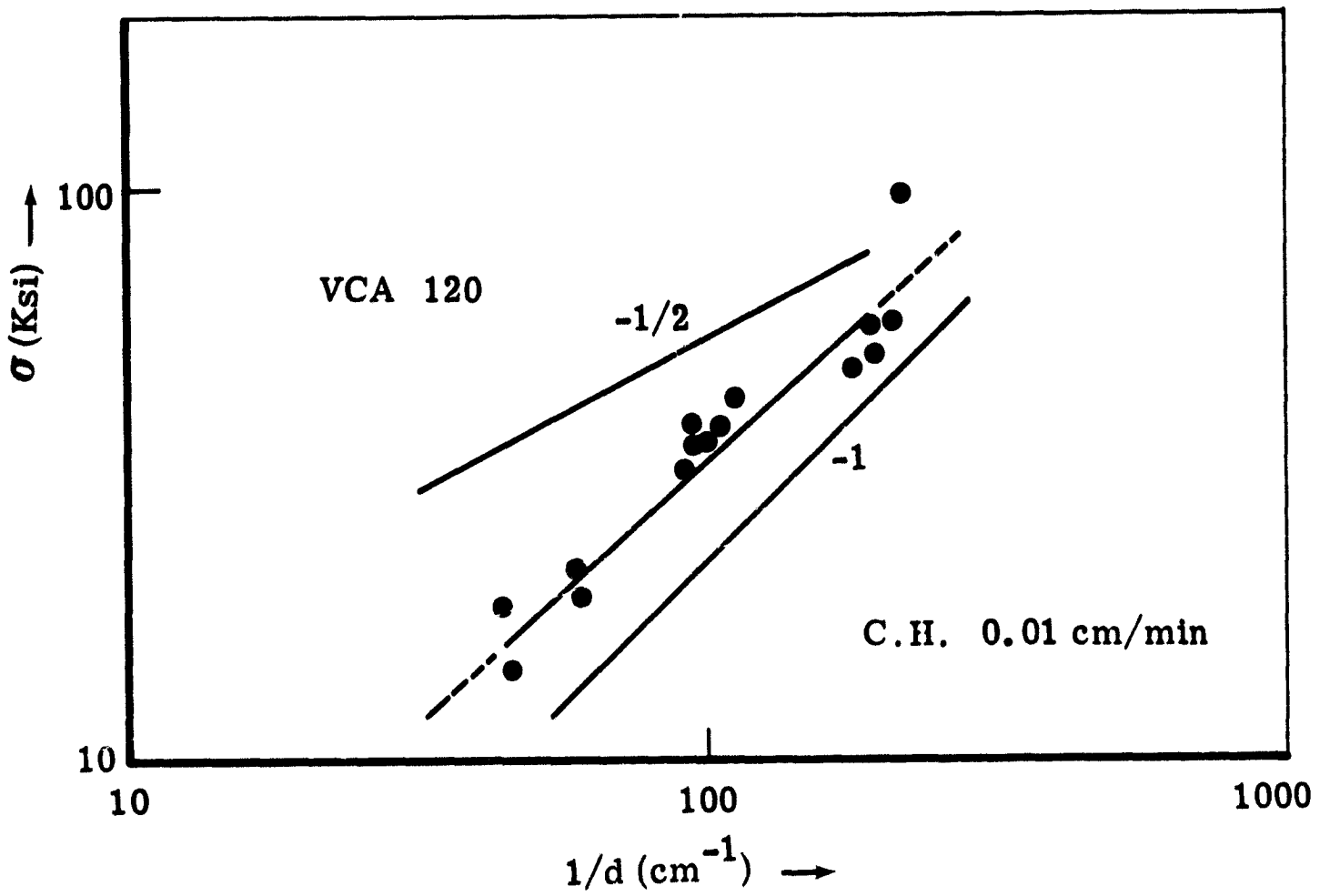

Fig. 21 Variation of net area initiation stress with grain size in Ti:13V:11Cr:3Al tested in 0.6M KCl at -500 mV.

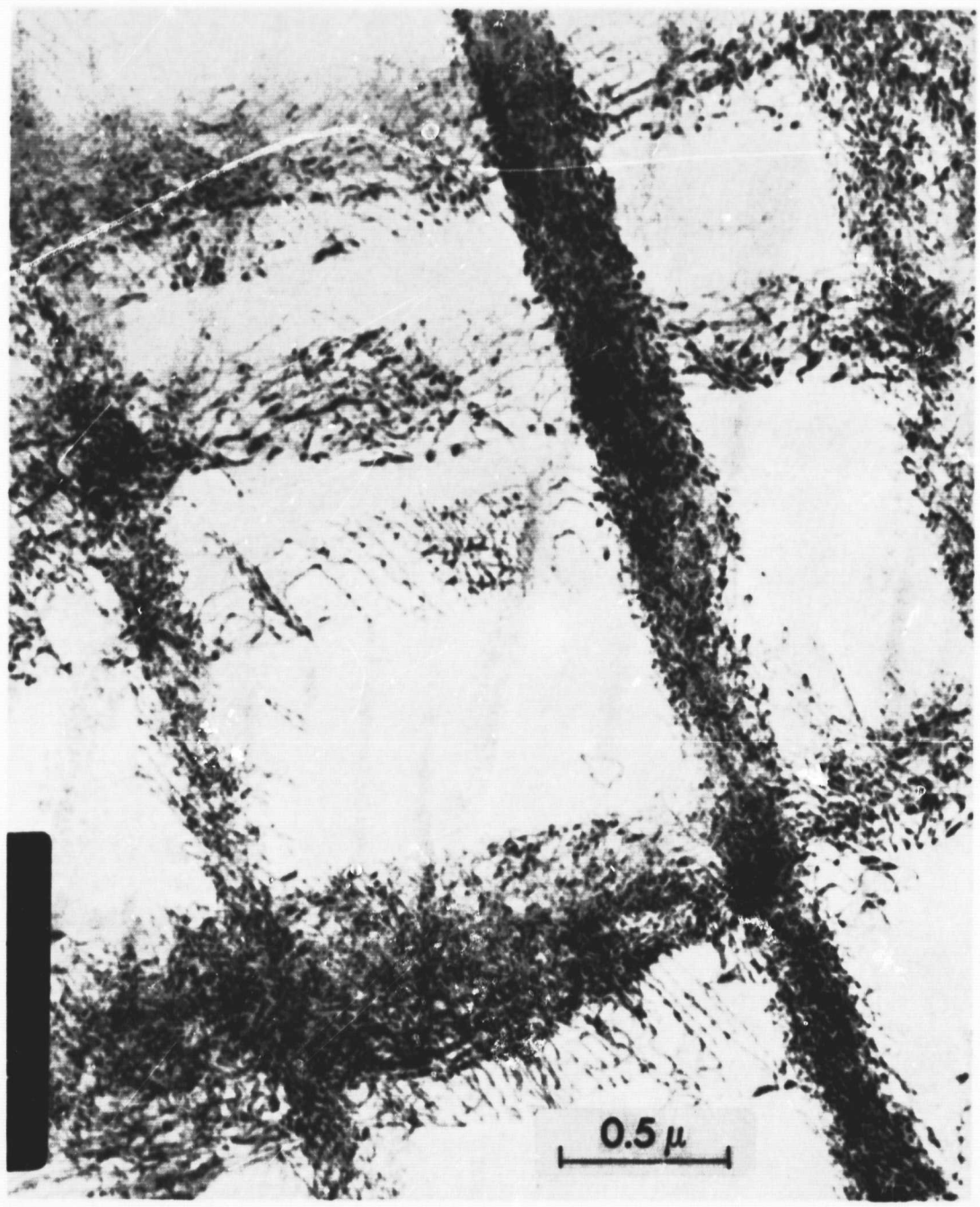

Fig. 22 Dislocation arrangements observed in Ti:13V:11Cr:3Al solution treated at 750°C, W.Q. and deformed ~4%, zone normal near [111].

Finally, it has been found that this alloy exhibits rather narrow and planar slip traces after deformation. The planar dislocation arrays observed in thin foils of deformed Ti:13-11-3 are shown in Fig. 22.

3.1.2 Discussion

Rather than discuss in detail the results reported above it is proposed to give a brief account of the metallurgical parameters which influence the aqueous SCC of titanium alloys. This account is by no means complete but it is considered that the factors listed below are at least recognizable if still in several cases qualitative.

A. Crystal Structure Examples of the four types of Ti alloys have been tested i.e., α, $\alpha+\beta$, $\beta+\alpha$ and β phase; in all cases the variation of initiation load (stress, K) and of SCC velocity with potential is the same. This indicates that the mechanism of SCC is independent of crystal structure.

B. Composition A critical alloy composition for the onset of transgranular SCC may be defined in some binary systems. In the Ti-Al system this is $\sim$5wt%Al and in Ti-Mn alloys is $\sim$10wt%Mn. In other systems the critical composition may not be defined accurately and many of the data are from relatively complex commercial alloys in which interactions between various alloying elements may be important. However, the following generalizations can be made: in α-phase alloys, Al, Sn and O increase susceptibility; for β-stabilized alloys, Mo appears to produce immunity

and from work on commercial alloys, most other β-stabilizing elements, e.g., V, Ta, Nb appear to produce immune β-phases; for β-eutectoid, Mn produces susceptible alloys and Cr and Fe are present in susceptible alloys; and Si and Cu appear to increase susceptibility to SCC (13).

C. Deformation and Mechanical Properties In all systems showing susceptibility to SCC, slip appears to occur by the movement of dislocations in narrow well defined slip bands. Deformation of Ti:Mo alloys is complex but does not occur by planar slip which may explain, in part, their immunity to SCC. In most cases the yield strength of the susceptible alloy (or phase in a multiphase system) is ≥100 Ksi. Ti:Al and Ti:O alloys with high solute concentrations fail by cleavage in the absence of an environment; it would be of interest to see if the same transition occurs in β-eutectoid systems such as Ti:Mn alloys. The exact significance of planarity of dislocation arrangements remain a matter of speculation. The "inner elastic zone" discussed in section 3.4 shows some promise of providing the answer but more work is required to make this a quantitative analysis. More information on rate effects, such as dislocation velocities etc. would also be of interest.

Finally, the strengthening processes in susceptible alloys are either due to solid solution strengthening or the formation of (ordered) coherent precipitates. Strengthening by other processes does not appear to increase susceptibility e.g. the ω-phase, and in some cases reduces susceptibility.

D. Influence of Microstructure and Heat Treatment

(1) The most important structures in titanium alloys, especially commercial alloys, are mixtures of the α & β phases. The case of most interest is if only one phase is susceptible to SCC, the cases where both or neither phases are susceptible is not considered here. The important parameters for $\alpha+\beta$ structures are

(a) Volume fraction of the susceptible phase - higher volume fraction increases susceptibility.

(b) Grain size - larger grain size increases susceptibility.

(c) Mean free path in susceptible phase - if there is a continuous path the alloy will be very susceptible. Surrounding the susceptible phase by the nonsusceptible phase can lower susceptibility.

(d) Defect structure in susceptible phase, e.g., the defect structures in tempered martensite appear to be beneficial.

The superiority of quenched (martensitic) and tempered structures over equiaxed structures in a α-rich alloy appears to arise from the factors (b) and (d).

(2) Martensitic Structures: The superiority of these structures over others in ($\alpha+\beta$) type susceptible alloys is due to probably three factors, small (plate) grain size, high defect density and the formation of a solid solution containing beneficial elements e.g. Mo and V. It should be noted that in α-phase type alloys although the martensitic structures show reduced susceptibility such structures are not immune. This is probably due to a larger plate size and lower defect density.

(3) Other Transformations: These must be considered individually as few generalizations can be made, e.g. ω-phase reduces influence of environment in Ti-Mn alloys but may increase susceptibility in A75 (high Fe which produces β-phase)(13).

The eutectoid system elements Cu and Si appear to increase susceptibilities from the work of Curtis (13) but it is not clear how this arises.

E. Fracture

In all cases examined in this study of failure under SCC conditions, the fracture surface contains some flat fracture; no examples of complete 45° (shear) failures have been found. In all cases of SCC failure examined of susceptible α and β phases, the fracture surfaces exhibits many features of cleavage failure. Further, it has been shown in both α-phase and β-phase[25] structures that failure occurs on a specific crystal plane. Other parameters that influence initiation such as notches and grain size also influence SCC failure in the same way as they do cleavage failure. Strain rate effects on initiation of SCC have been studied to some extent and two trends may be distinguished. Firstly, Curtis et al., (13) have shown that in some alloys there are differences between K_{1SCC} measured in specimens loaded in solution and specimens loaded in air and then the solution added. From these results it would appear that in a susceptible alloy system e.g. Ti-Al the variation may be represented diagrammatically as in Fig. 23. Secondly, in the past years it has been observed that the rate of loading appears to influence the initiation load for SCC. In the alloy Ti:8-1-1

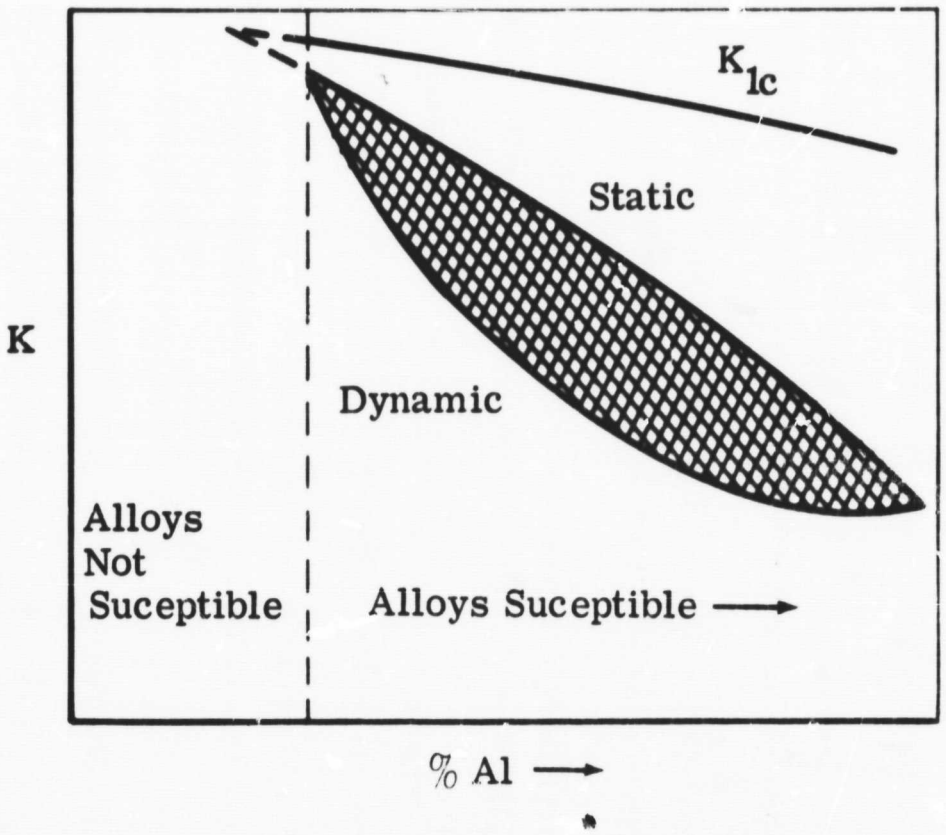

Fig. 23 A diagramatic representation of the influence of aluminum content and type of loading on the measured K_{1SCC} value.

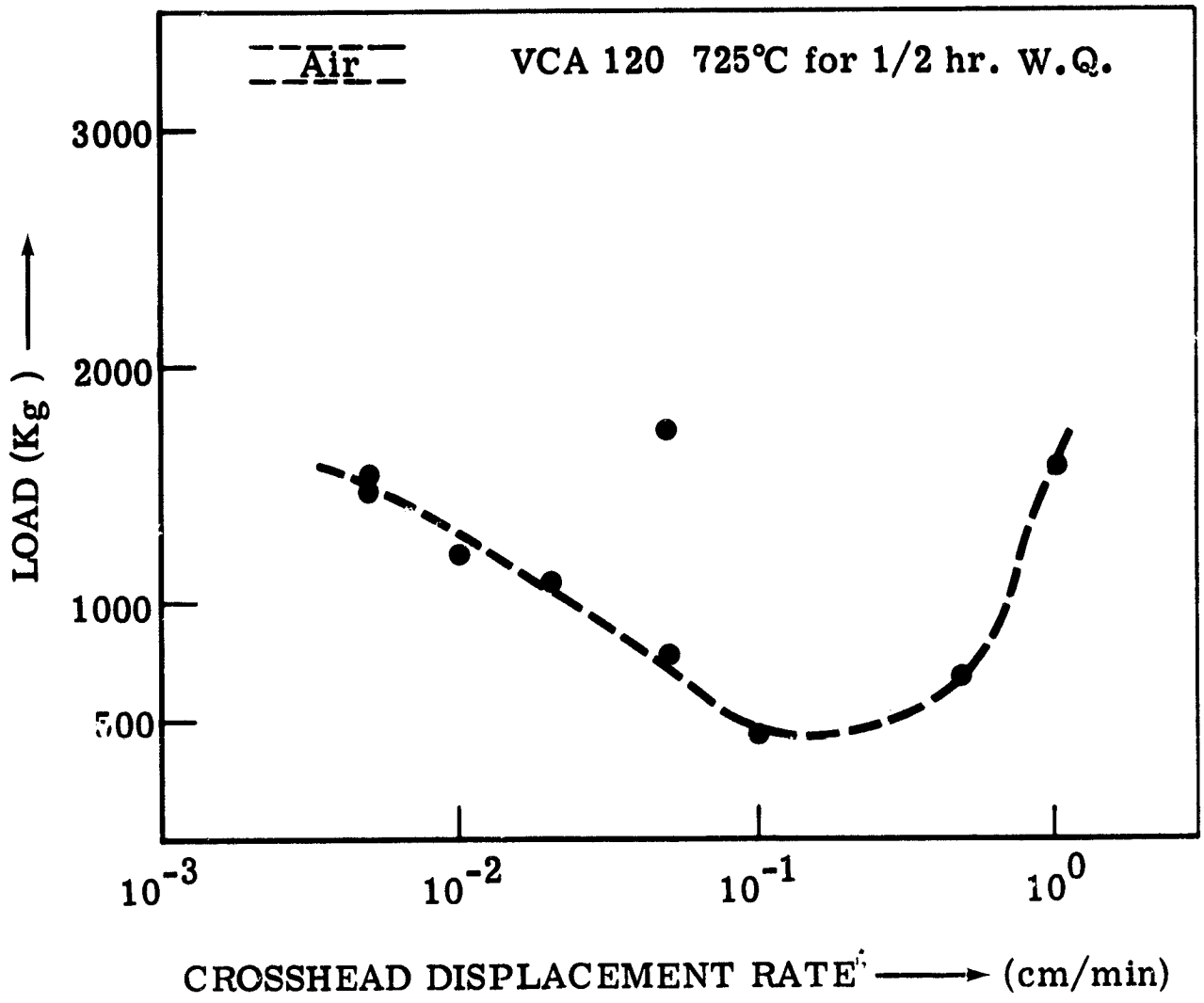

Fig. 24 Variation of initiation load with cross head displacement rate in Ti:13V:11Cr:3Al tested in 0.6M KCl at -500 mV.

the effect is not large but in the Ti:13-11-3 alloy, heat treated just above the β-transus, the initiation load shows a large variation with strain rate. This is shown in Fig. 24 from which it can be seen that at slow and fast strain rates, the initiation load is high but at intermediate rates quite low values are observed. It should also be noted that in this series of tests and in others the scatter at these intermediate rates is quite large.

F. Mechanism

All evidence obtained in this laboratory indicates that the basic mechanism outlined in previous reports, i.e., the interaction of halide ions with atoms at the crack apex to produce a cleavage (like) fracture, is correct. The results on hydrogen charging indicate that, although the presence of the element may influence the nucleation of SCC cracks, it does not influence their growth to a large extent. Further, the velocities of cracking observed under slow strain rate hydrogen embrittlement condition are several orders of magnitude slower than SCC cracks. The kinetics of cracking also appear inconsistent with the formation of gross hydride particles needed for the fast strain rate hydrogen embrittlement. Thus we must conclude that if hydrogen is involved in the embrittlement (SCC) mechanism it must be due to a hitherto unknown interaction of hydrogen with Titanium. Specific criticisms of the hydrogen mechanism include:

(a) SCC does not occur in solutions known to introduce hydrogen into titanium alloys - notably acid fluoride solutions;

(b) SCC occurs in solution which does not contain hydrogen, e.g. CCl_4;

(c) The electrochemical mass-transport-kinetic model indicates that hydrogen ions should migrate away from the crack tip.

3.2 SCC of Aluminum Alloys

3.2.1 The Influence of Stress on the Velocity of Stress Corrosion Cracks in Aluminum Alloys

We measured the influence of the applied crack tip stress intensity on the propagation rate of stress corrosion cracks in high strength aluminum alloys, using three different types of specimens:

(a) Single-edge-crack tension specimens (SEN)

(b) Tapered double-cantilever-beam specimens (TDCB)

(c) Straight double-cantilever-beam specimens (DCB)

As the crack grows during a stress corrosion test, each specimen type causes a different and characteristic variation of the stress intensity as a function of the crack length:

(a) In SEN specimens, the stress intensity increases as the SCC crack grows. Finally, the stress intensity reaches a critical value, K_{Ic} or $K_{I\delta}$, where catastrophic (mechanical) failure sets in. Our SEN specimens were stressed in an Instron tensile machine. We made use of the following K-calibration (27):

$$K_I = Y \frac{P\, a^{\frac{1}{2}}}{B\, W} \qquad (1)$$

where a = crack length, P = load, B = thickness of the specimen, W = width of the specimen, and

$$Y = 1.99 - 0.41(a/W) + 18.70(a/W)^2 - 38.48(a/W)^3 + 53.85(a/w)^4 .$$

(b) In TDCB Specimens, the stress intensity is constant over a limited fraction of the specimen width. Our TDCB specimens were stressed with dead-weights in a specially built jig. Crack tip stress intensities were calculated from the applied load and the specimen geometry, using the methods given in the literature (19, 28, 29).

(c) In DCB specimens, the stress intensity decreases as the crack growths, provided the crack tip is not too close to the specimen end. Consequently, the crack always remains stable, its propagation rate decreases and finally becomes too small to be measurable. Our DCB specimens were self-stressed and bolt-loaded, similar to those described in recent reports (16, 30, 31). Stress intensities were calculated from deflections at the load line, specimen geometry and crack length, using the following equation:

$$K_I = \frac{\delta E h \left[3h(a + 0.6h)^2 + h^3\right]^{\frac{1}{2}}}{4\left[(a + 0.6h)^3 + h^2 a\right]} \qquad (2)$$

where δ = deflection at the load line, E = Young's modulus, h = the beam height and a = crack length.

Results from all three kinds of SCC-specimens are compared in Figs. 25, 26 and 27. For this comparison, the specimens have been made from the commercial aluminum alloy 7039 in the -T6 condition. (Table 6 gives the chemical composition and the designation of all the aluminum alloys we tested.)

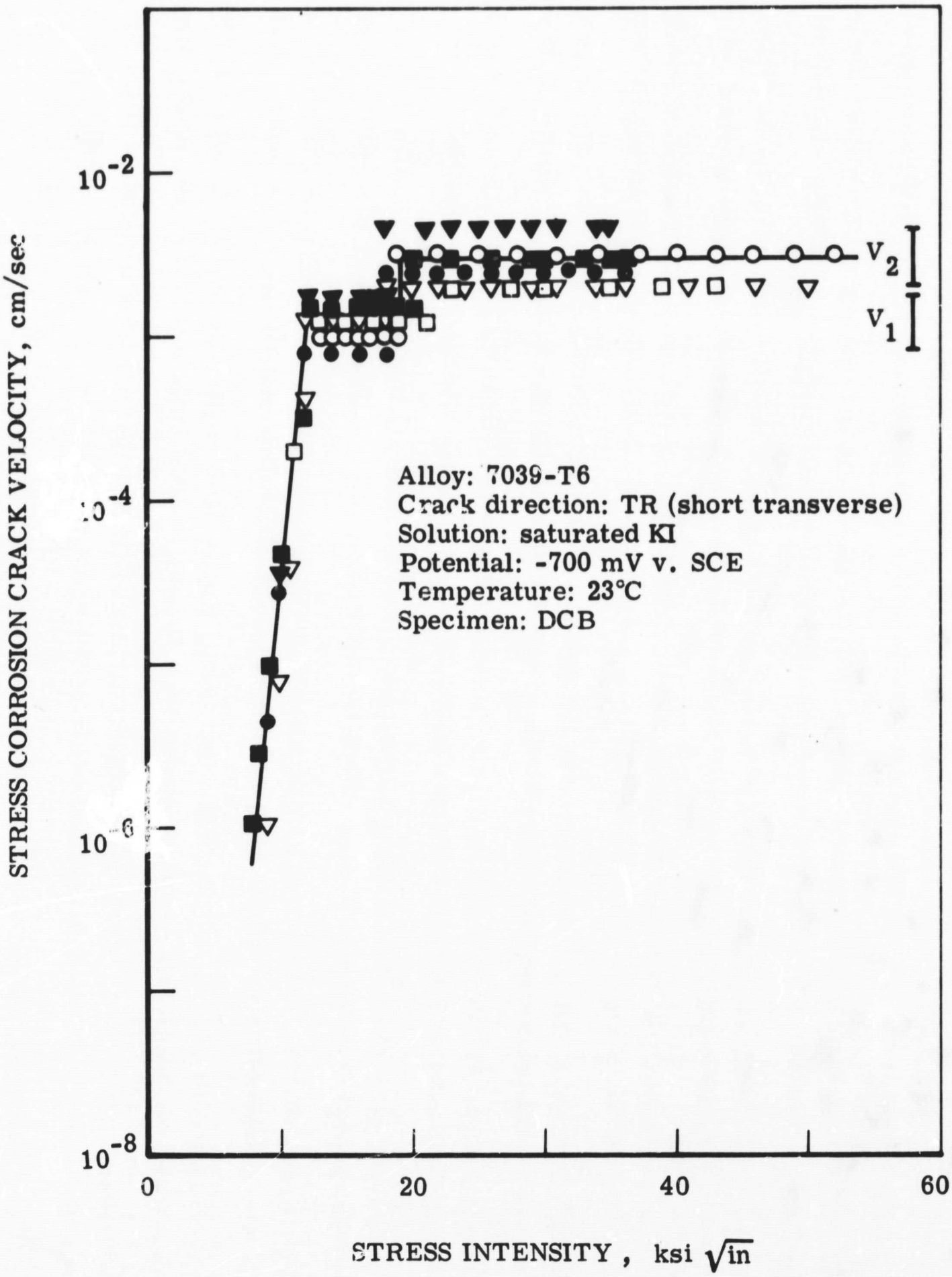

Fig. 25 Crack tip velocity as a function of the applied stress intensity. Results from six DCB specimens of two different 7039-T6 plates (open symbols and closed symbols).

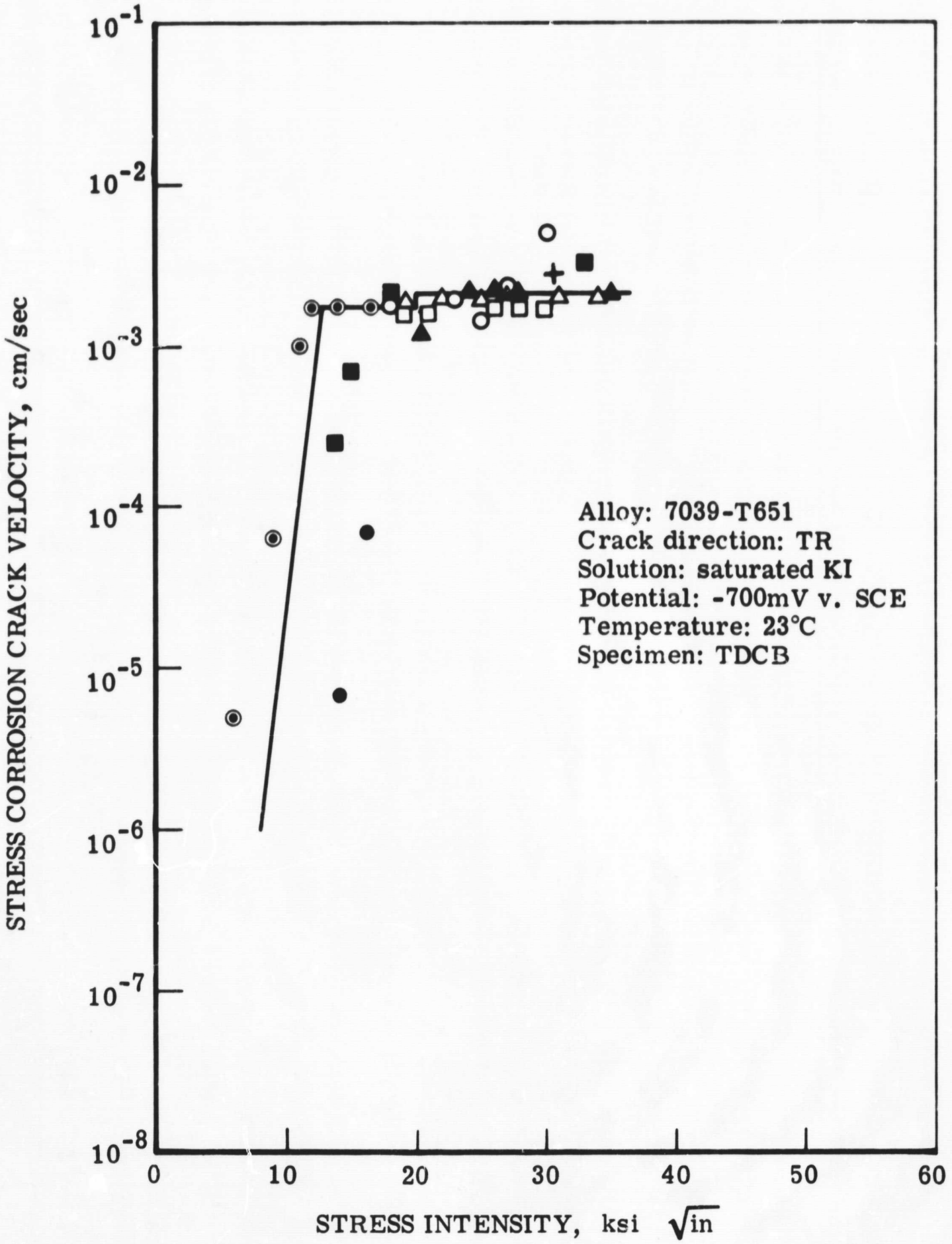

Fig. 26 Crack tip velocity as a function of the applied stress intensity. Results from eight TDCB specimens.

Table 6 Chemical Composition of the Aluminum Alloys Investigated

alloy	composition, wt.-%								
	Zn	Mg	Cu	Cr	Si	Fe	Mn	Ti	Al
7039 - T6	4.0	2.8	0.1	0.2	0.3	0.4	0.2	0.1	balance
7075 - T651	5.6	2.5	1.6	0.25	0.4	0.5	0.3	0.2	balance
7079 - T651	4.3	3.3	0.6	0.2	0.3	0.4	0.2	0.1	balance
Al-Mg2,5-Zn6	5.87	2.50	0.001	0.00	0.002	--	0.002	0.00	balance

Fig. 25 shows the results of six SCC experiments with DCB-specimens made from two different 7039-T6 plates. Fig. 26 gives the results from eight TDCB specimens of the same alloy. The experimental points in Fig. 27 come from tests using SEN specimens, while the solid lines are those of Fig. 25 and Fig. 26, inserted in Fig. 27 for comparison. All tests were carried out at 24 $\pm$ 1°C in saturated aqueous KI solution at a potential of -700 mV versus the saturated calomel electrode.

From the results presented here (and from over 200 more tests we have made to date), the influence of the stress intensity on the SCC-crack velocity can be described as follows:

Over a wide range of stress intensities, the velocity of SCC-cracks is <u>independent</u> of the applied crack tip stress intensity (region II). In other words, the velocity versus stress intensity curve has one or two plateaus of constant velocity (in this report called v_1 and v_2). Below a certain stress intensity level, however, the SCC-crack velocity is strongly stress dependent (region I).

The experimental determination of the stress-dependent part of the velocity versus stress intensity curve is very time-consuming. Therefore, we usually stopped our tests when the velocities dropped below 10^{-6} cm/sec. In some cases we measured cracks as slow as 10^{-8} cm/sec, but even then the cracks never really stopped, they just grew slower as the stress intensity decreased. Thus, for the high strength aluminum alloys we tested, there appears to be no physical meaning to K_{ISCC}, a limiting stress intensity below which SCC cracks

"do not propagate". The measurement of such a limit would be indicative only of the patience of the investigator. At present, the comparison of the stress corrosion behaviour of two different aluminum alloys requires the measurement of the full velocity versus stress intensity curves. As we learn more and more about such functions, it will perhaps be possible in the future to again describe the susceptibility to SCC of an aluminum alloy by a single number (or two numbers), such as: The slope and position of the stress dependent part of the velocity versus stress intensity curve, or the stress intensity (and velocity) where the stress-dependent and the stress independent parts meet. Work in progress in this laboratory is designed to clarify this point.

Stress intensity determinations from SEN and DCB tests are reproducible with good accuracy as, for example, can be seen from the small degree of scatter in the stress dependent part of the velocity-versus-stress-intensity curve in Fig. 25. TDCB specimens lead to much more scatter at small K-values as is apparent from Fig. 26. For this and other (mainly economic) reasons, dead-weight loaded TDCB specimens appear to be inferior to the self-stressed DCB specimens and the SEN tension specimens. Thus, in the latter part of this investigation the TDCB specimen type was abandoned.

Nevertheless, the use of TDCB specimens has had one specific advantage: It showed that the stress <u>in</u>dependent part of the velocity-versus-stress-intensity-curve is <u>not</u> due to a particular combination of decreasing K and increasing pH at the crack tip, as one might deduce from DCB tests alone (30).

This conclusion is corroborated by the observation of stress independent v-versus-K curves under increasing stress intensity (SEN) as well as under decreasing stress intensity (DCB) (Fig. 25 and 27).

Fig. 28 shows the crack velocity versus stress intensity curve for a 7075-T651 high-strength aluminum alloy. This result, together with the following from still other aluminum alloys shows that the shape of the velocity-versus-stress-intensity curve described above is a fairly general one in aluminum-base alloys. It appears therefore that the velocity of a stress corrosion crack in aluminum alloys is limited by at least two different mechanisms: one dependent on the applied stress, the other independent of it.

3.2.2 The Influence of Halide Ion Concentration on the Velocity of Stress Corrosion Cracks in High Strength Aluminum Alloys

We observed a striking analogy between the influence of halide ion concentration on the propagation rate of stress corrosion cracks in aluminum alloys and titanium alloys. These alloys differ completely in chemical composition. They also differ in stress corrosion cracking: SCC cracks in aluminum alloys are always intercrystalline, in titanium alloys (e.g. Ti:8-1-1), they are transcrystalline. Despite these differences, we found that in both alloy systems

Cl^-, Br^-, I^-, -ions promote SCC

(i.e., their presence increases the SCC crack tip velocity)

F^- -ions are SCC inhibitors

(i.e., their presence reduces the crack tip velocity when compared to that in distilled water).

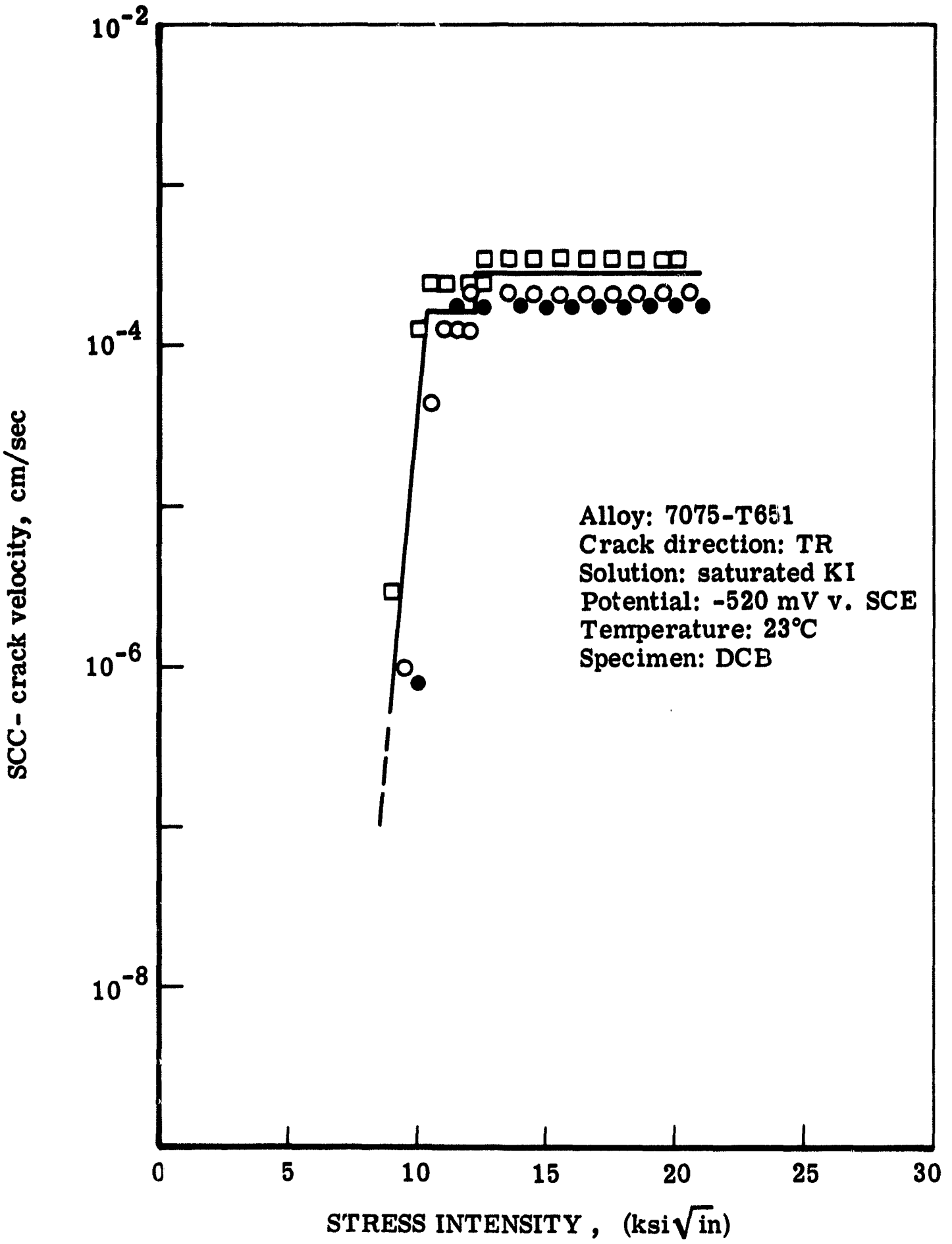

Fig. 28 High-strength commercial alloy 7075-T651; the function of SCC-velocity versus stress intensity resembling that of Fig. 25. Results from 3 DCB specimens.

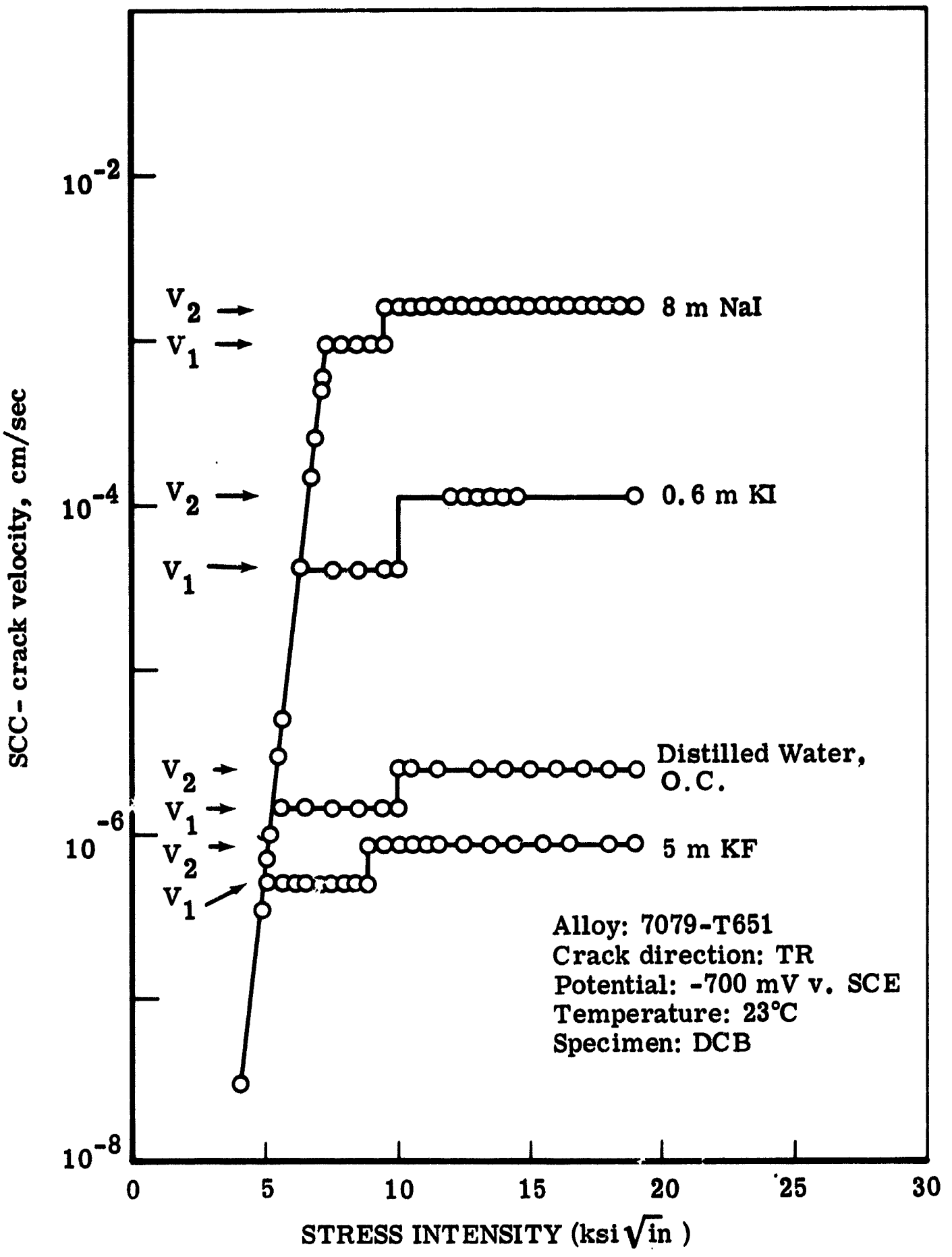

Fig. 29 Crack tip velocity in the commercial aluminum alloy 7079-T651 as a function of electrolyte composition and applied stress intensity.

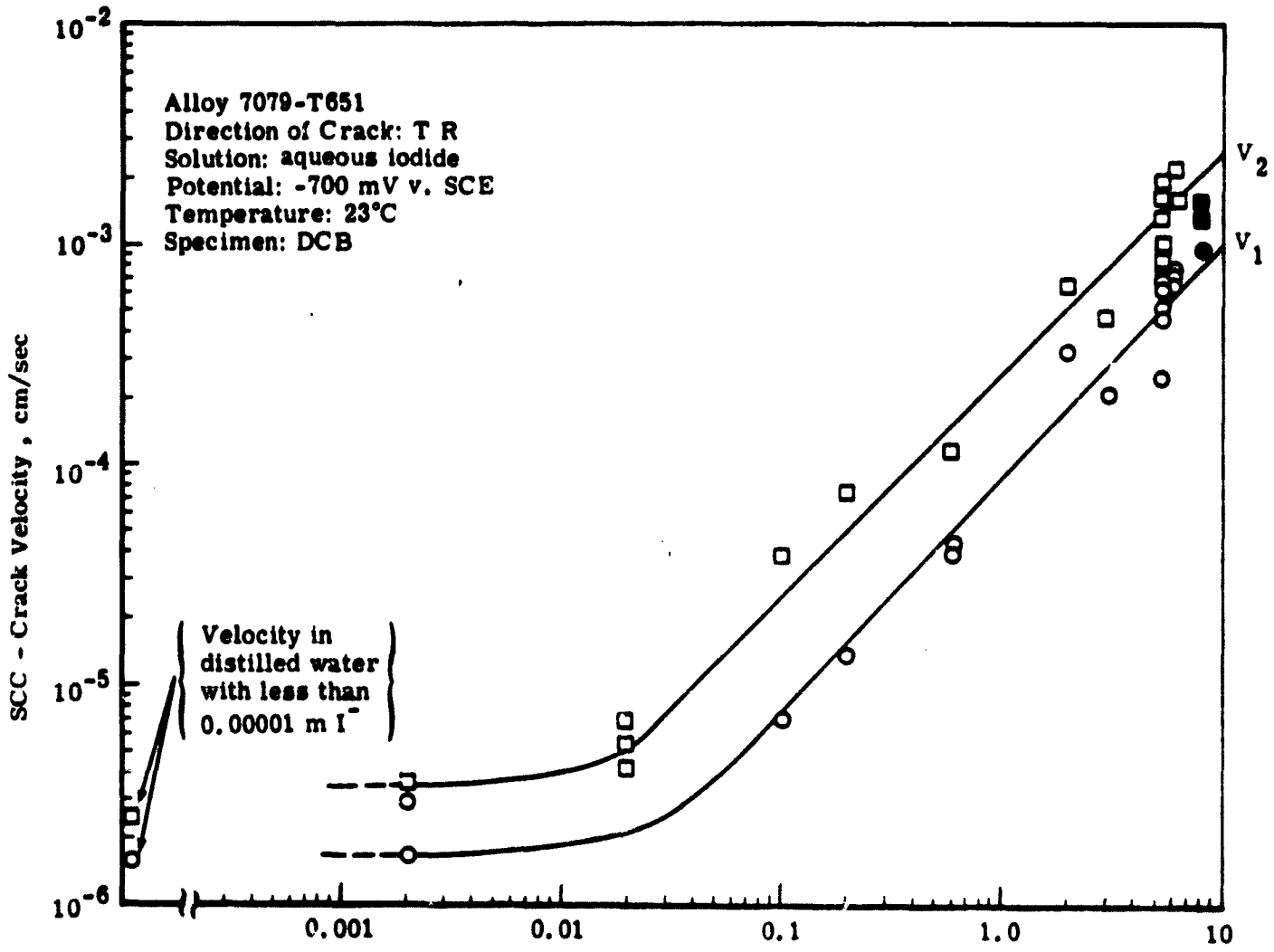

Fig. 30 Commercial aluminum alloy 7079-T651. Variation of velocity with iodide concentration in the electrolyte.

This is illustrated in Fig. 29 which gives crack velocities of the commercial aluminum alloy 7079-T651 as a function of stress intensity in different solutions (Note that the shape of the curves is very similar to those shown above for other aluminum alloys, Figs. 2?-28). In both, distilled water and aqueous 5 m KF solutions, SCC cracks were very slow but clearly measurable. The presence of fluoride reduced the crack velocity by a factor of more than two. The addition of chloride, bromide or iodide, on the other hand, increases the velocity up to a thousand times, depending on temperature, electrochemical potential, stress, and bulk electrolyte concentration. The influence of the iodide concentration on the SCC crack propagation rate in 7079-T651 at constant temperature and potential is illustrated in Fig. 30. This illustration shows the concentration dependence of the stress independent parts, v_1 and v_2, of the velocity-versus-stress-intensity curves. (The influence of the halide ion concentration on the stress dependent part is very small, if any, and could not be measured in aluminum alloys to date.)

Fig. 30 shows that the relationship between crack velocity and iodide concentration is linear over almost three orders of magnitude. This significant result is discussed further in Section 3.4. At concentrations lower than 0.01 Mol/liter, there is almost no influence of concentration on SCC crack velocity and the nearly horizontal curve is easily extrapolated to the velocities measured in distilled water. Again, here is a similarity to titanium alloys, where the velocity-versus-concentration curve also consists of a horizontal and a steeper increasing branch (see Fig. 38). The scatter

of the many experimental results in 5.5 molar solution gives a fair indication of the limits of the accuracy of our best testing methods (namely the DCB) when applied to different specimens. For one and the same specimen, the accuracy is much higher.

The knowledge of the influence of electrolyte concentration on SCC crack velocity is important for the study of the fundamental aspects of SCC as well as for the design of accelerated SCC tests for applied purposes. It was thus desirable to measure this function for a quite different alloy too. We used a high purity ternary aluminum-magnesium-zinc alloy. Since this alloy was recrystallized and had equiaxed grains, cracks would not propagate in the desired symmetry plane of DCB specimens. Therefore we resorted to SEN specimens.

Examples of the resulting velocity-versus-stress-intensity curves are given in Fig. 31. The stress independent parts v_1 and v_2 are clearly distinguished. Their concentration dependence is shown in Fig. 32. Again, the velocity depends linearly on the iodide concentration within the limits of our experimental accuracy. This indicates that such linearity may be fairly general, since the results shown in Fig. 30 and Fig. 32 come from alloys that differ not only in chemical composition (see Table 6), but also in heat treatment and grain shape: The 7079-T651 alloy was at maximum hardness and had extremely flat and straight grain boundaries in the crack direction, while the Al-Mg2.5-Zn6 alloy was in the underaged condition and had equiaxed grains with an average diameter of 0.5 mm.

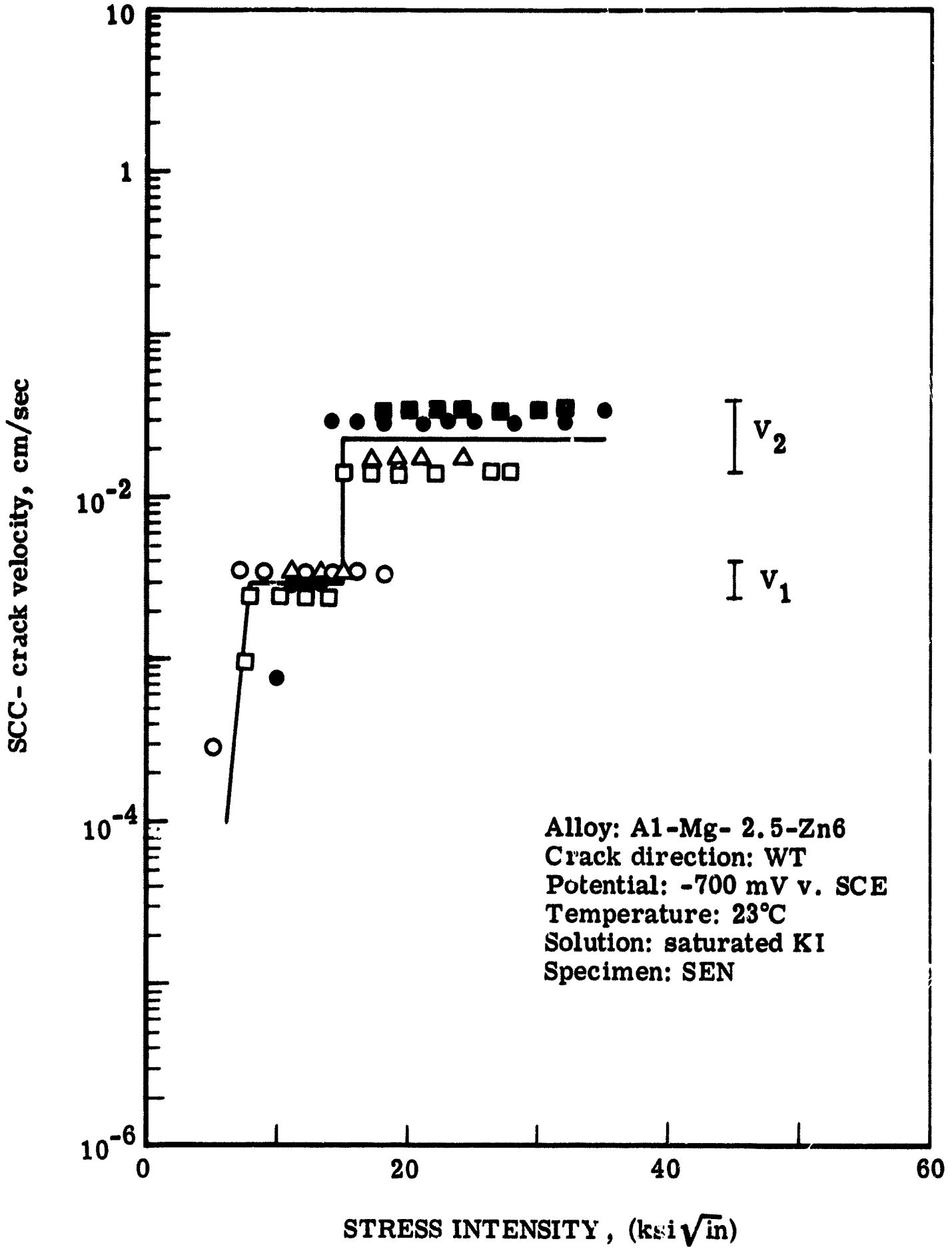

Fig. 31 High-purity ternary aluminum-magnesium-zinc alloy. Influence of stress intensity on velocity of cracks.

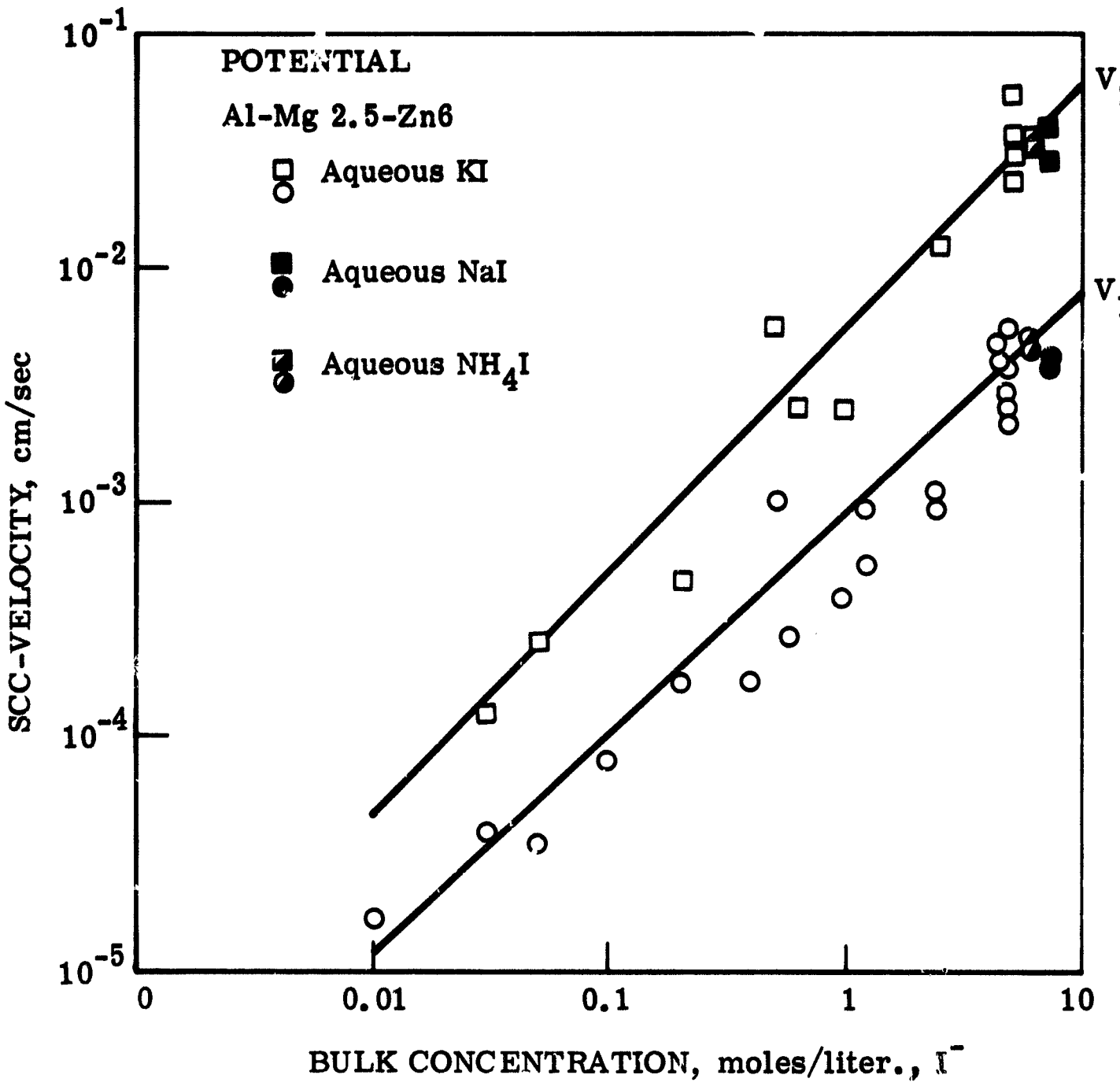

Fig. 32 High-purity ternary aluminum-magnesium-zinc alloy. Variation of velocity with iodide concentration in the electrolyte.

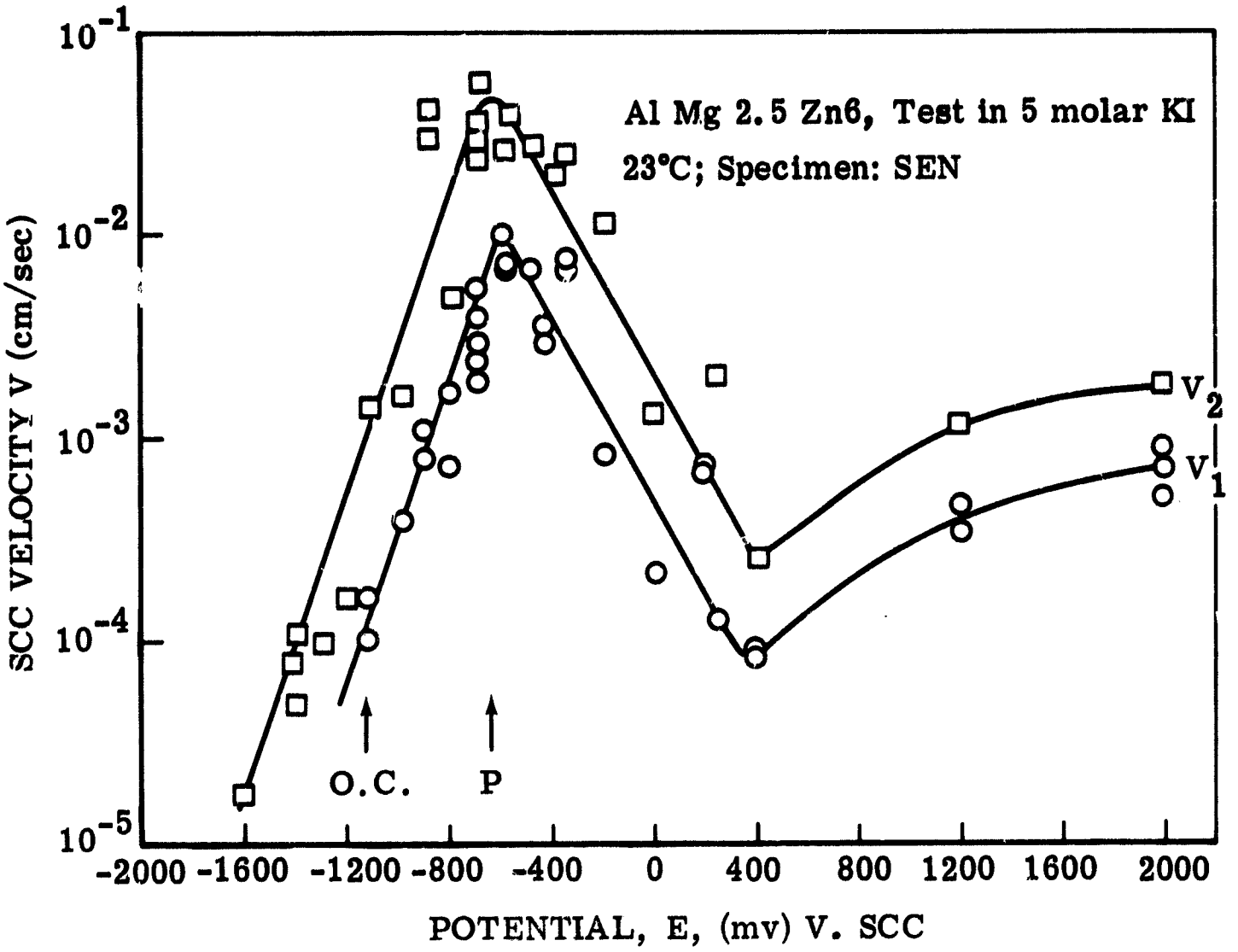

Fig. 33 Variation of SCC-crack velocity with potential. High-purity ternary aluminum-magnesium-zinc alloy. SEN-specimens.

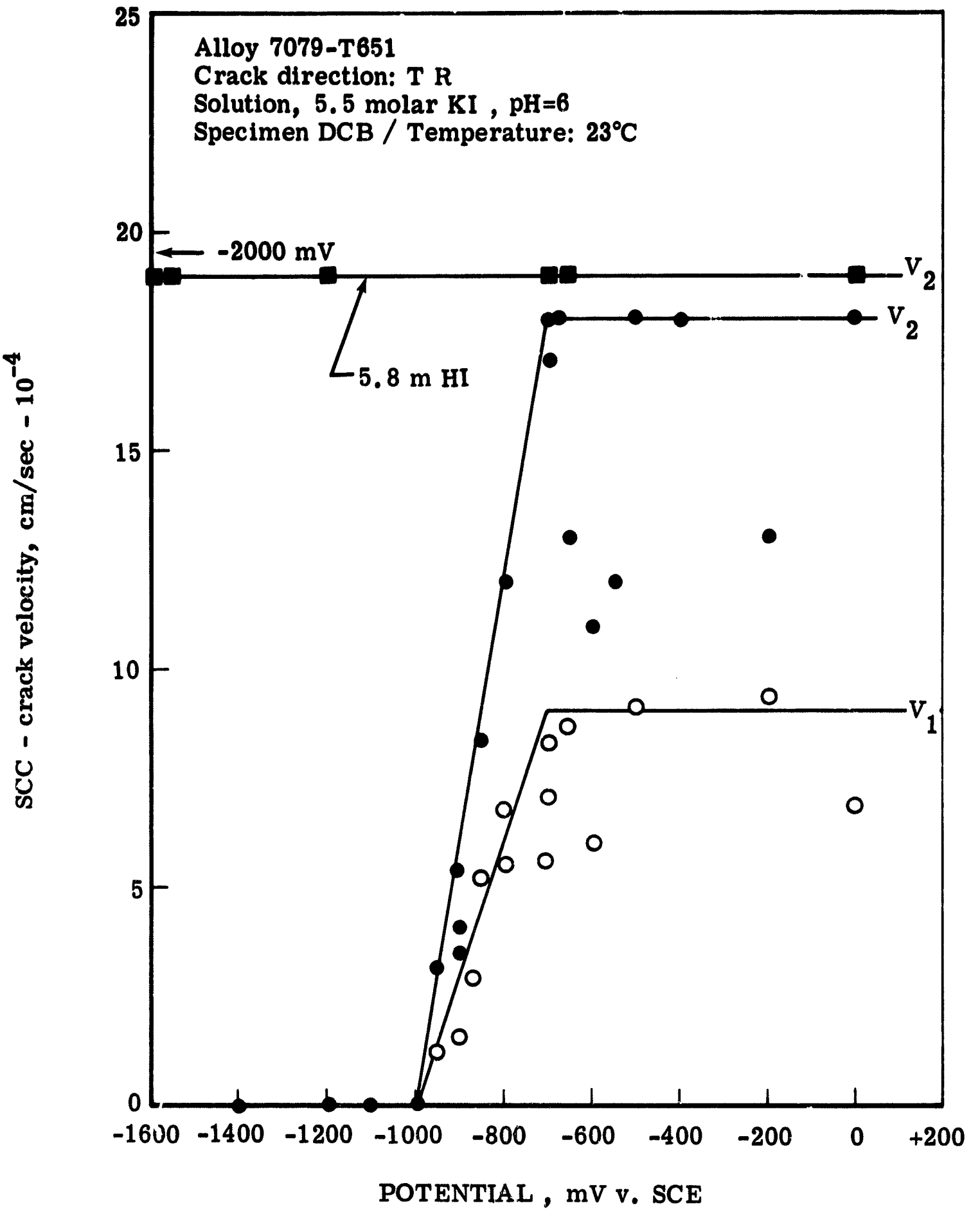

Fig. 34 Variation of velocity with potential in neutral and in strongly acidic iodide solutions. Commercial aluminum alloy 7079-T651, DCB-specimens.

A comparison of Fig. 30 and 32 reveals that SCC cracks in the high purity alloy are about ten times faster than in the commercial alloy. This could be due to any of the differences just mentioned. The influence of the microstructure on crack propagation rate is being further studied in this laboratory.

3.2.3 The Influence of Electrochemical Potential on the Velocity of Stress Corrosion Cracks in Aluminum Alloys

The velocity of crack propagation in high strength aluminum alloys varies with applied potential in a similar way to that previously observed in titanium (1). As shown in Figs. 33 and 34, velocity increases with potential from a potential more negative than the open-circuit (O.C.) or mixed potential to the pitting potential (P.). Above the pitting potential the velocity is constant or decreases as with titanium (6). Test results of the high-purity alloy (using SEN specimens, Fig. 33), spanned nearly four decades, indicating that in neutral aqueous halide solutions, potential is one of the major influential parameters on SCC. The scatter of these tests however was too great to say with certainty whether velocity is an exponential function of potential or whether there are linear regions as with titanium. DCB tests with the commercial aluminum alloy 7079-T651 give results of higher accuracy. According to Fig. 34, there is indeed a region where the maximum velocity measured depends linearly on potential as with titanium. We found that this relation between velocity and potential depends on stress, alloy composition and

and the concentration of hydrogen ions present in the bulk of the electrolyte.

In neutral aqueous iodide solutions, cathodic protection is effective at potentials more negative than -1000 mV v. SCE, as shown in Fig. 34. In strongly acidic solutions however, the influence of potential on velocity is nil, as one can also see from Fig. 34. When the pH is lowered from 6 to between 0 and -1, cathodic protection becomes impossible. This again is paralleled in titanium alloys as shown in Section 3.1 of this report.

3.2.4. Influence of Viscosity of the Electrolyte on the Velocity of SCC-cracks in Aluminum Alloys

From the electrochemical mass-transport-kinetic model for stress corrosion cracking (21) (see also section 3.4 of this report), it could be expected that viscosity should be an important parameter controlling the velocity of cracking. Specifically, variations of viscosity should have the same influence on velocity as variations of the halide ion concentration. Thus, for aluminum alloys we expect a linear relation between crack velocity and viscosity of the electrolyte. To check this prediction, a series of experiments has been conducted with a 7079-T651 aluminum alloy in 3-molar KI-solution, the viscosity of which was varied by varying the percentage of glycerol in the glycerol-water solvent. The results are shown in Fig. 35.

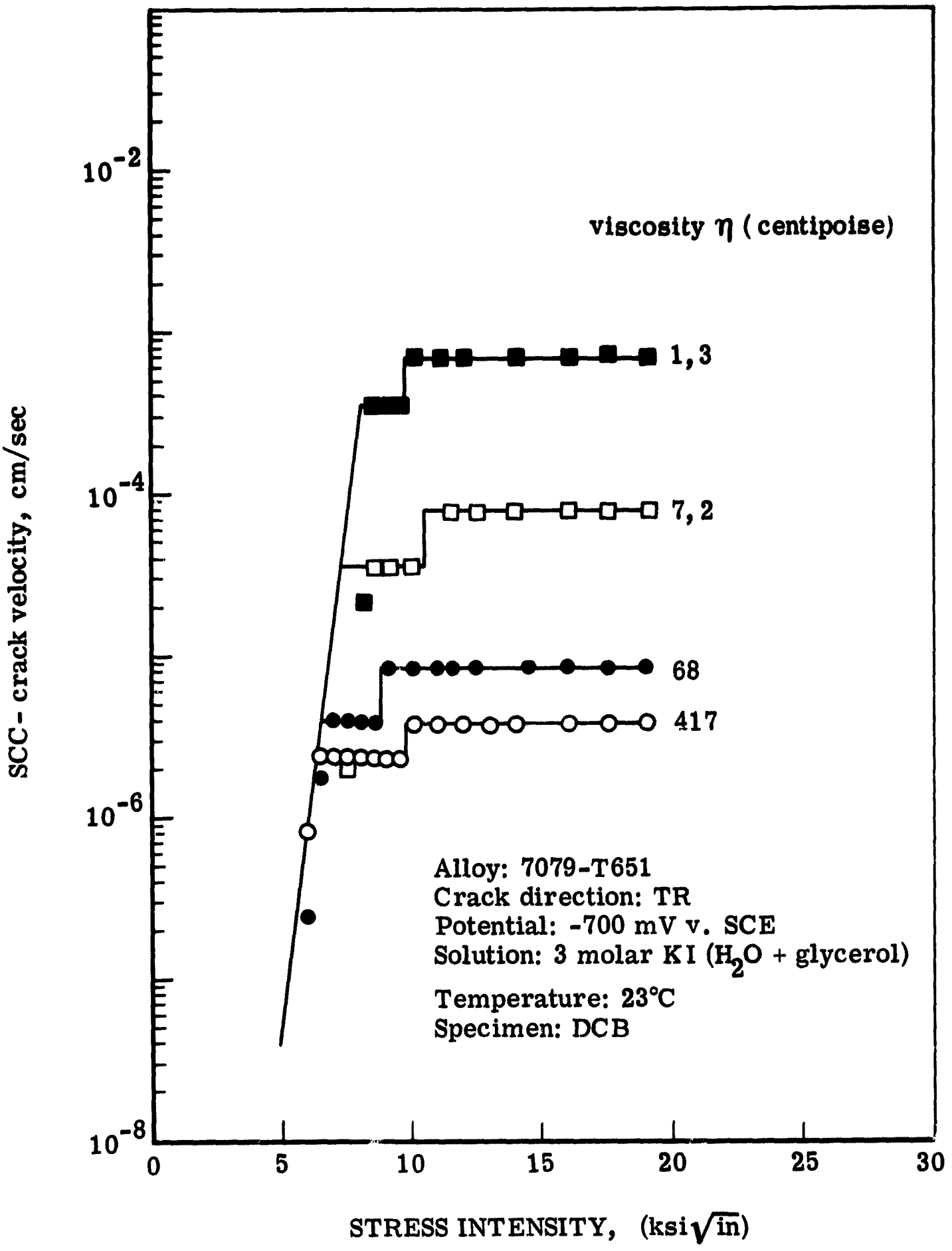

Fig. 35 Influence of viscosity and stress intensity on SCC crack velocity of a commercial high-strength aluminum alloy.

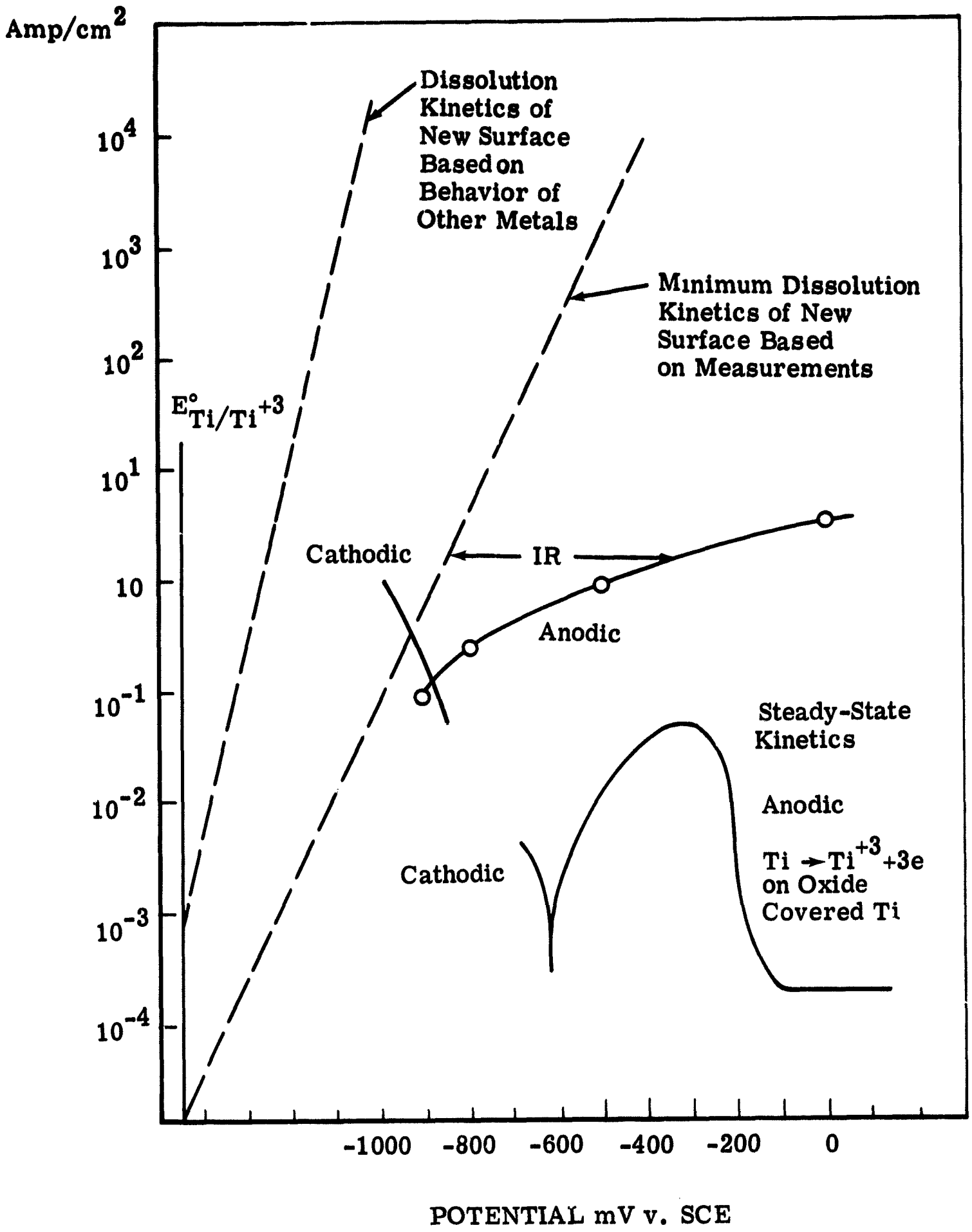

Fig. 36 Kinetic data for oxidation of new titanium surface and steady-state kinetics in 12M HCl.

It appears that viscosity indeed is an important parameter controlling the velocity of cracking. A discussion of these results and a comparison with results from titanium alloys and with theoretical expectations is given in section 3.4 of this report. As can be seen from Fig. 35, variations of viscosity affect only the stress independent part of the velocity-versus-stress-intensity curve. The stress dependent part is not affected by viscosity within the limits of the experimental accuracy of $\pm$ 1 ksi$\sqrt{\text{in}}$. This is consistent with the explanation offered below which indicates that the velocity in the stress dependent part is kinetically limited rather than mass transport limited.

3.3 Polarization of Titanium and Its Alloys in HCl

Polarization curves were made of various titanium alloys in concentrated HCl to determine if there was any significant difference in their electrochemistry that could be correlated with their SCC behavior. Steady-state polarization curves were measured as a rapid screening tool although these data may bear little relation to the events on fresh surface near the crack tip.

Fig. 36 shows a steady-state polarization curve of Ti:8-1-1 in 12 M HCl. Although a typical active-passive behavior is observed in concentrated HCl solutions, the current density in the active region is orders of magnitude lower than the anodic current density observed for freshly generated surfaces. Anodic kinetic data reproduced from Fig. 10, Ref. 4, for new Ti:8-1-1 surfaces in 12M HCl are shown in Fig. 36 for comparison. At the

time that these data were obtained it was thought that this anodic current was for formation of oxide but it is now known that it is predominantly for formation of Ti^{+3}(11). The dashed line is for Tafel Kinetics with an arbitrary 120 mv slope, the correction for IR drop being approximately

$$\Delta\phi_{IR} = \frac{i\Delta X}{\kappa} \qquad (3)$$

which for a current density of 1 amp/cm^2, a Luggin capillary-to-electrode spacing of 0.3 cm and a 12 M HCl conductivity of 0.5 Ω^{-1} cm^{-1} gives a potential drop of 0.6 volts. This Tafel line then represents a minimum kinetic limit for new surface.

That the steady-state anodic kinetics data are at least five orders of magnitude lower than those for new surface indicates that even in the active region a considerable passivation exists. This passivation is very likely caused by oxide which, according to the potential - pH diagram shown in Fig. 2, Ref. 11, can exist in a metastable equilibrium in strongly acid solution. Steady-state dissolution of titanium in the active region may proceed through an oxide formation and dissolution step.

Steady-state rate of dissolution of pure titanium in the active region is very strongly dependent on HCl concentration as shown in Fig. 37. The curves are similar to data of Otsuka (32). Steady state was fairly quickly reached in 12 M HCl but very slow to attain in 6 M HCl. In contrast, the peak anodic current for Ti:8-1-1 fractured in 12 M HCl and for commercially pure titanium fractured in 3 M HCl were very similar, both being limited by IR drop. This means that the kinetics of dissolution of the fresh surfaces

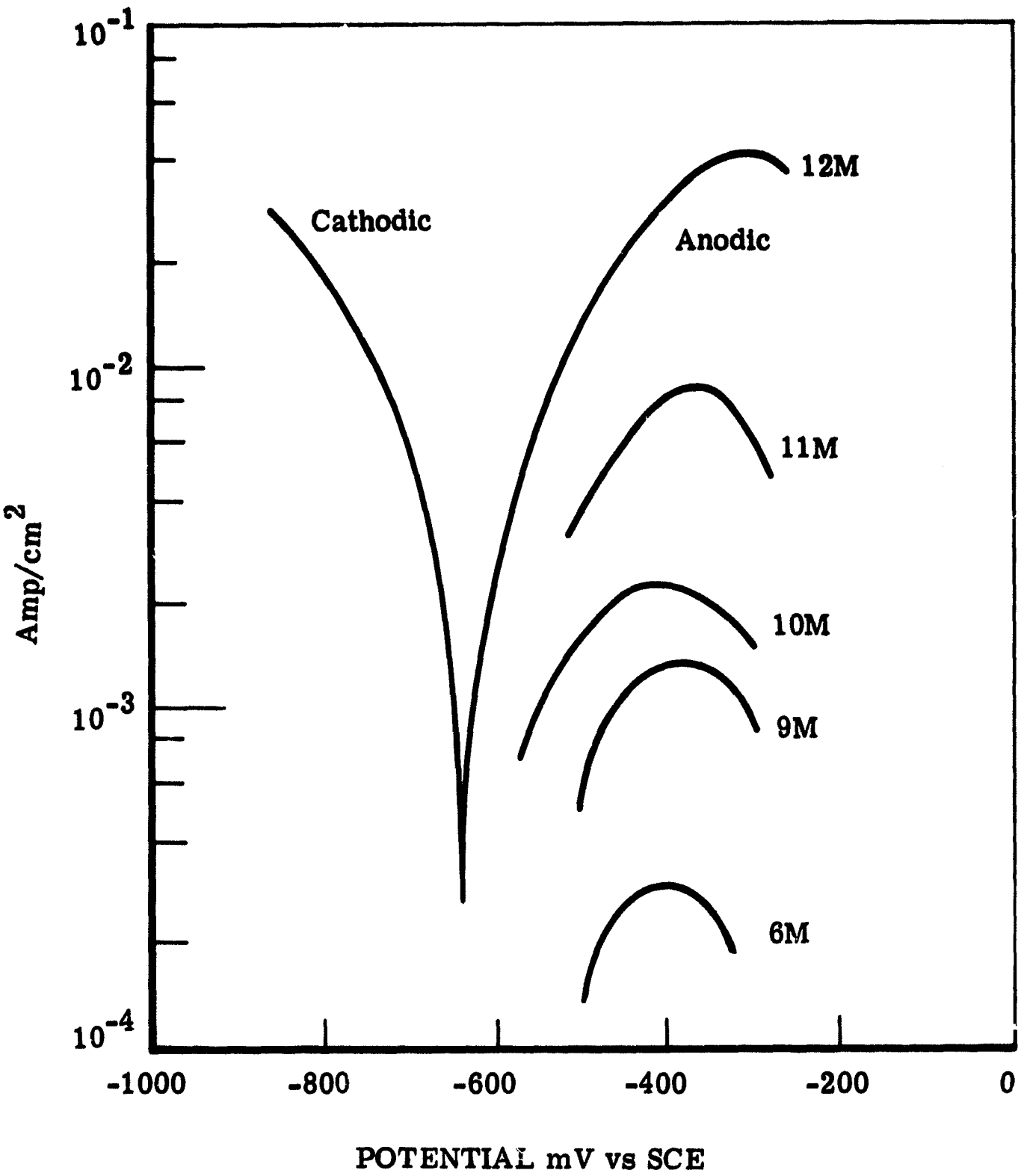

Fig. 37 Steady-state kinetic data for titanium in HCl solutions.

have not as yet been measurable. At high overpotentials the IR drop becomes limiting, at low overpotentials hydrogen evolution obscures, and the bare surface is rapidly covered with oxide. A Tafel line, with an $i_o = 10^{-3}$ amp/cm^2 and a 60 mv slope typical for dissolution of many non-passivating metals, is shown for comparison in Fig. 36 to the minimum dissolution rate from the kinetics experiments.

Anodic polarization curves were run for various titanium alloys in 12 M HCl. The shape of the curve in the active region was for the most part the same but there were some shifts in the maximum current as indicated in Table 7. Within the accuracy of the data there appeared to be no strong trend with aluminum composition up to 16 weight percent. Manganese alloys showed a distinct increase in corrosion rate, while Ti:14 Mo did not give an active corrosion region. The non-susceptibility to SCC of the Ti:Mo alloy (11) which has the same structure as the Ti:Mn alloy may possibly be related to this difference in electrochemistry, although it is not clear how because the steady-state behavior would not be expected near the crack tip.

It is planned to make kinetic measurements on fresh surfaces of the alloys to determine if differences also occur under these conditions.

Table 7 Maximum Current Density in Active Region for Titanium and Alloys in 12 M HCl

	i_{max} (ma/cm^2)
Zone refined Ti	37
Iodide Ti	32
Ti:3Al	38
Ti:8½Al	39
Ti:16Al	40
Ti:8-1-1	42
Ti:8Mn 650°C 1 week	64
Ti:8Mn 950°C WQ - 400	83
Ti:8Mn 900°C WQ	90
Ti:16Mn	420
Ti 14Mo	0

3.4 Correlation of Titanium and Aluminum SCC Data

In this section the effect of concentration, viscosity and stress concentration factor on SCC velocity in titanium and aluminum will be compared to predictions of the electrochemical mass-transport-kinetic model.

The relation of SCC velocity in titanium and aluminum alloys to bulk concentration of halide is shown in Fig. 38. The dashed line is for the mass transport limited case for the formation of a single monolayer of halide in the tip zone (6) given by the equation

$$V = \frac{z_- F D_- \gamma C^\circ_-}{2nQ_x \ell n(\ell/\delta P)} \qquad (4)$$

where n = 1 for a monolayer. Values of the other parameters are given in Table 8. That the titanium data were above the dashed line and had a smaller slope was attributed to recycling of halide within the crack due to displacement by oxide (6). An approximate model for halide displacement made possible by some simplifying assumptions such as a constant time required for the halide displacement gave the equation (6),

$$C = \frac{2n\left(1 + \frac{D_H}{2D_-}\right)Q_x}{F\gamma D_H} V\ell n\, V/V^s \qquad (5)$$

which is as shown as the dashed curve in Fig. 38. This equation approximated the asymptotic behavior of the velocity in dilute solutions and was considered to be a reasonable explanation of the results (6).

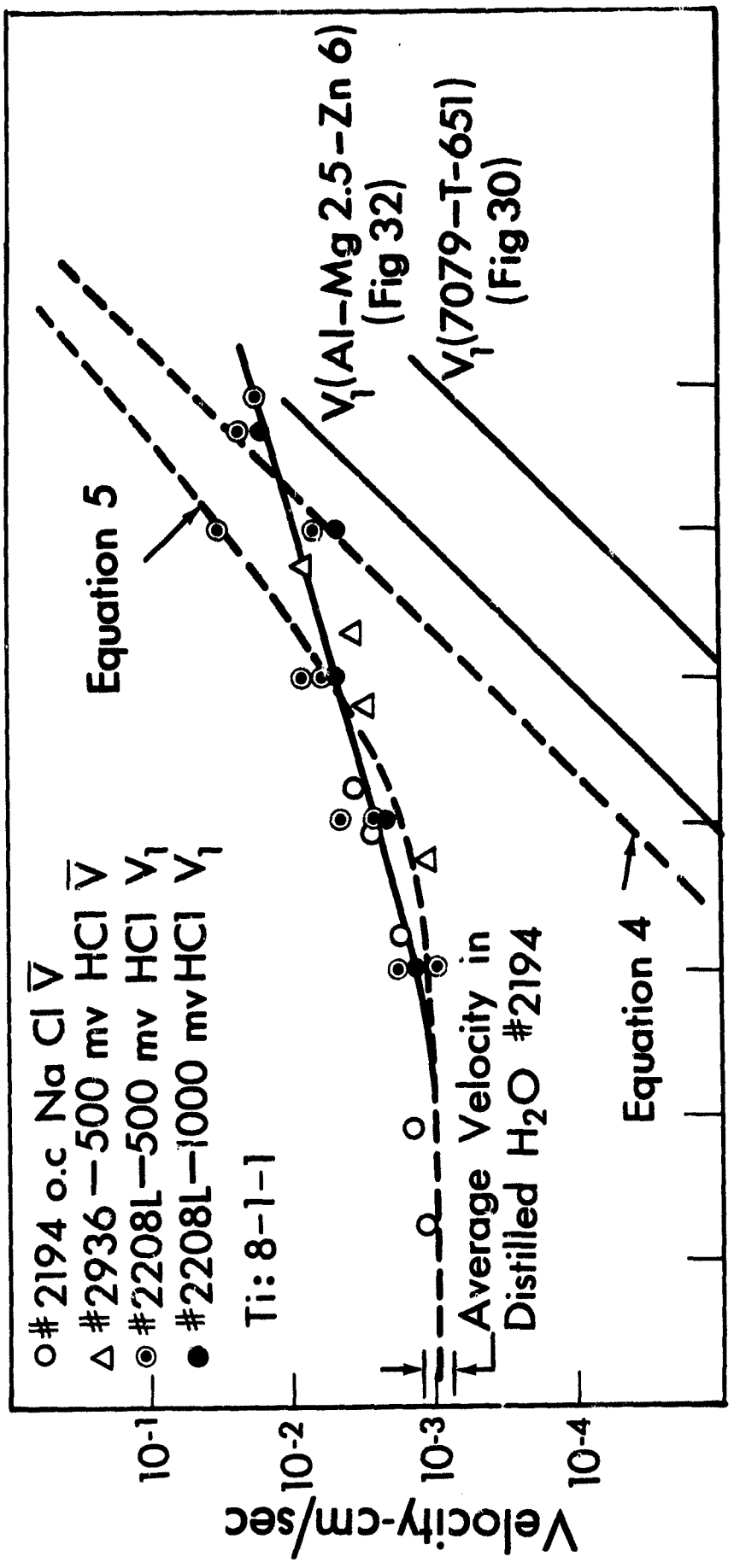

Fig. 38 Correlation of crack propagation velocity with halide ion concentration.

Table 8 Values of Parameters used in Equations 4 and 5

z_-	=	1 equiv/mole
F	=	96,500 coul/equiv
D_-	=	1×10^{-5} cm^2/sec
D_H	=	6×10^{-5} cm^2/sec
γ	=	0.05
n	=	1 for titanium
Q_x	=	425×10^{-6} $coul/cm^2$
ℓ	=	10^{-1} cm
δ^p	=	10^{-6} cm
V^s	=	10^{-3} cm/sec for titanium

The velocity data for aluminum (V_1 from Figs. 30 and 32) are below the dashed line for equation 4 but parallel to it. The simplest way to account for this is to assume that more than a monolyaer of halide is formed in the tip zone and that the halide is not displaced by oxide within the distance, ℓ. The distance, ℓ, is defined as the position at which current and solution flow in from the sides of the crack, or about 0.1 to 1 specimen thickness. The slower displacement by oxide with aluminum is consistent with a smaller pH range of stability of the oxide near neutral pH (33) as compared to titanium.

That a monolayer of halide appears to be formed in the tip zone with titanium and greater than 10 monolayers with aluminum bears a curious resemblance to data of Robertson and Gani (34) for gaseous adsorption of chlorine on titanium and aluminum. They found that at low pressures of chlorine gas the adsorption was extremely rapid on a clean surface of titanium up to a monolayer, followed by a slow uptake. In other words the first monolayer inhibited further growth. In the case of aluminum, the reaction was rapid up to fourteen monolayers before slowing down. It is a mystery, however, why this phenomena should apparently carry over to the aqueous solution in the tip zone.

The effect of changing viscosity of the electrolyte with glycerol on SCC velocity in titanium and aluminum also appeared to be consistent with predictions from equations 4 and 5 as will be shown here. Diffusivity of nondissociating solutes can be approximately related to viscosity by the relation (35).

$$D_{AB} = 7.4\times10^{-8} \frac{(\psi_B M_B)^{\frac{1}{2}} T}{\mu \tilde{V}_A^{\,0.6}} \qquad (6)$$

It will be assumed for the present purpose that tnis relation can also be applied to dissociated species such as hydrogen ions and chloride ions. It will be assumed that the factor $(\psi_B M_B)^{\frac{1}{2}}$ is constant in glycerol-water solutions because the higher molecular weight of glycerol is partially offset by a smaller value of ψ_B. The possible change for the hydrogen ion from a Grothus mechanism in water to a purely viscous drag mechanism in glycerol will also be ignored. The three orders of magnitude change in viscosity from pure water to glycerol justify neglect of these second order effects. The diffusivities of hydrogen ion and chloride ion will therefore be expressed as

$$D = D_o \frac{\mu_o}{\mu} \qquad (7)$$

Substituting equation 7 in equations 4 and 5 and rearranging gives

$$V = \left[\frac{z_- F D_- \mu_o \gamma C^\circ_-}{2n Q_x \ell n\ (\ell/_\delta P)}\right] \frac{1}{\mu} \qquad (8)$$

and

$$\mu = \frac{F\gamma D_o \mu_o}{2n\left(1 + \frac{D_{Ho}}{2D_{-o}}\right) Q_x V \ell n(V/V^s)} \qquad (9)$$

Equations 8 and 9 are plotted in Fig. 39 and compared to the experimental data for titanium and aluminum. The values of n chosen were one for titanium and 30 for aluminum consistent with the observations on the effect of concentration on velocity. The slopes of the experimental data plots were remarkably close to that predicted by the equations; approximately $-\frac{1}{2}$ for titanium and -1 for aluminum. The absolute values of the velocity for titanium were higher than that predicted by the equation consistent with earlier observations (higher by up to a factor of six in mill annealed specimens as compared to duplex annealed specimens and the model (6)). This remarkable fit of the data and model equations is considered rather strong support of the electrochemical mass transport limited SCC velocity concept.

The requirement that n = 30 for aluminum to get equation 8 to fit the experimental data in Fig. 39 has important implications regarding the mechanism at the crack tip. This indicates almost without doubt that there is electrochemical reaction in the tip zone and that electrochemical reaction at the tip is very likely. However, the fact that n = 1 gives the best fit for titanium does not allow distinguishing between an adsorption phenomenon or an electrochemical reaction at the tip. The hydrogen and oxide mechanisms at the tip have previously been eliminated in the MTK model for titanium in aqueous solutions (21).

The very rapid kinetics of dissolution of fresh titanium surfaces shown in Fig. 36 though are consistent with the high SCC velocities observed. For example, the highest velocity observed in titanium is about 10^{-1} cm/sec, which when put into the equation

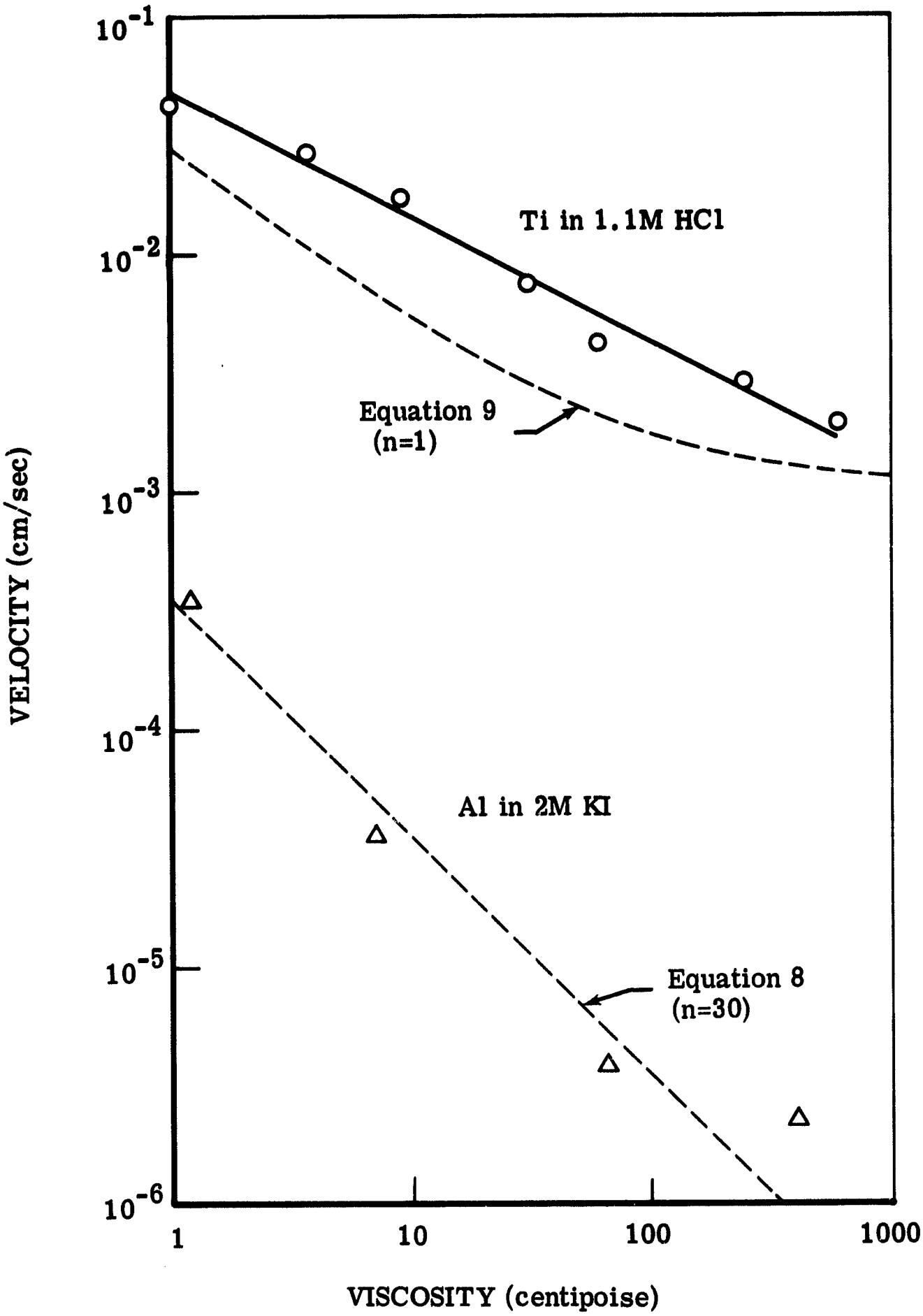

Fig. 39 Correlation of crack propagation velocity with viscosity of H_2O-glycerol solutions.

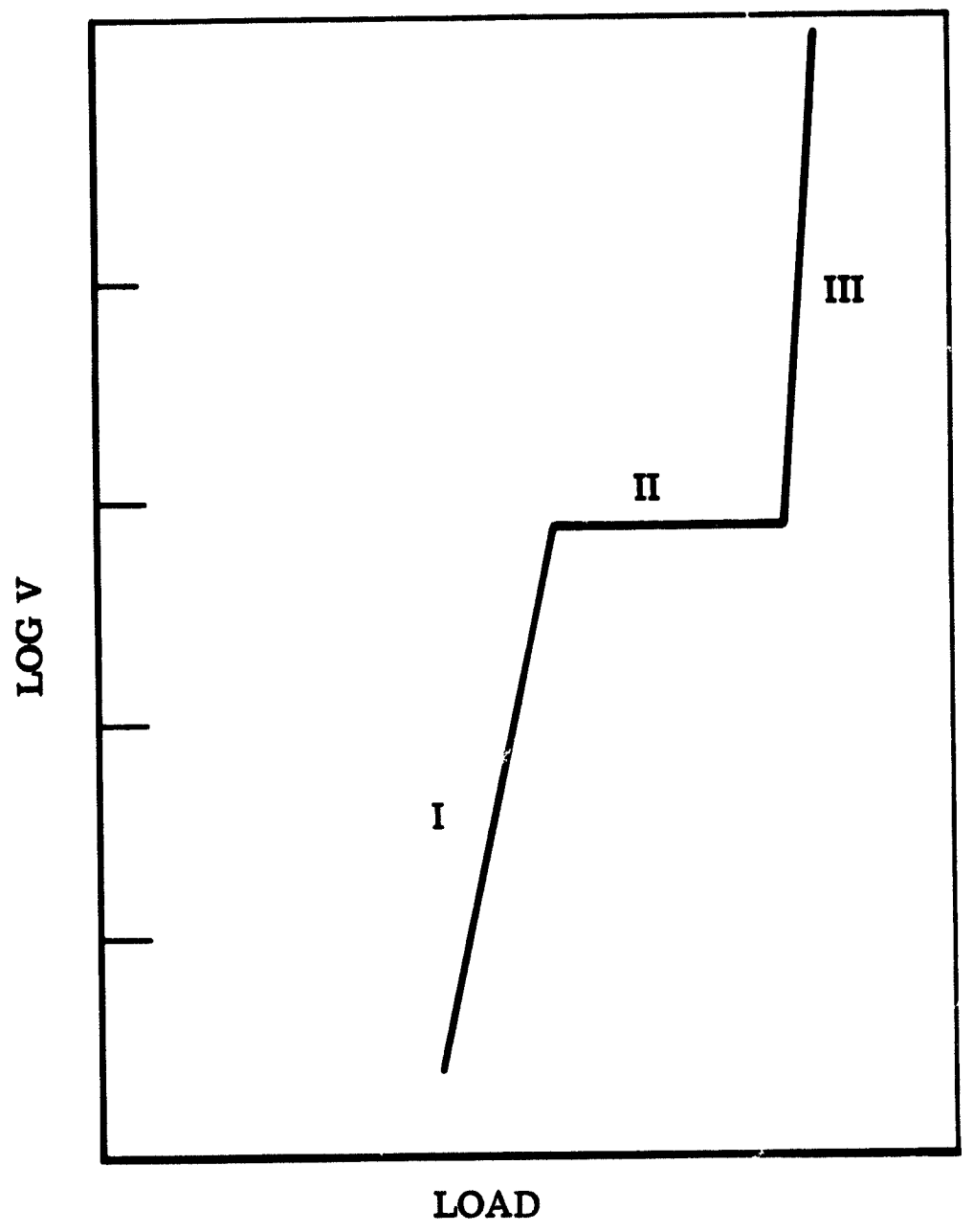

Fig. 40 Regions of crack propagation velocity as a function of load.

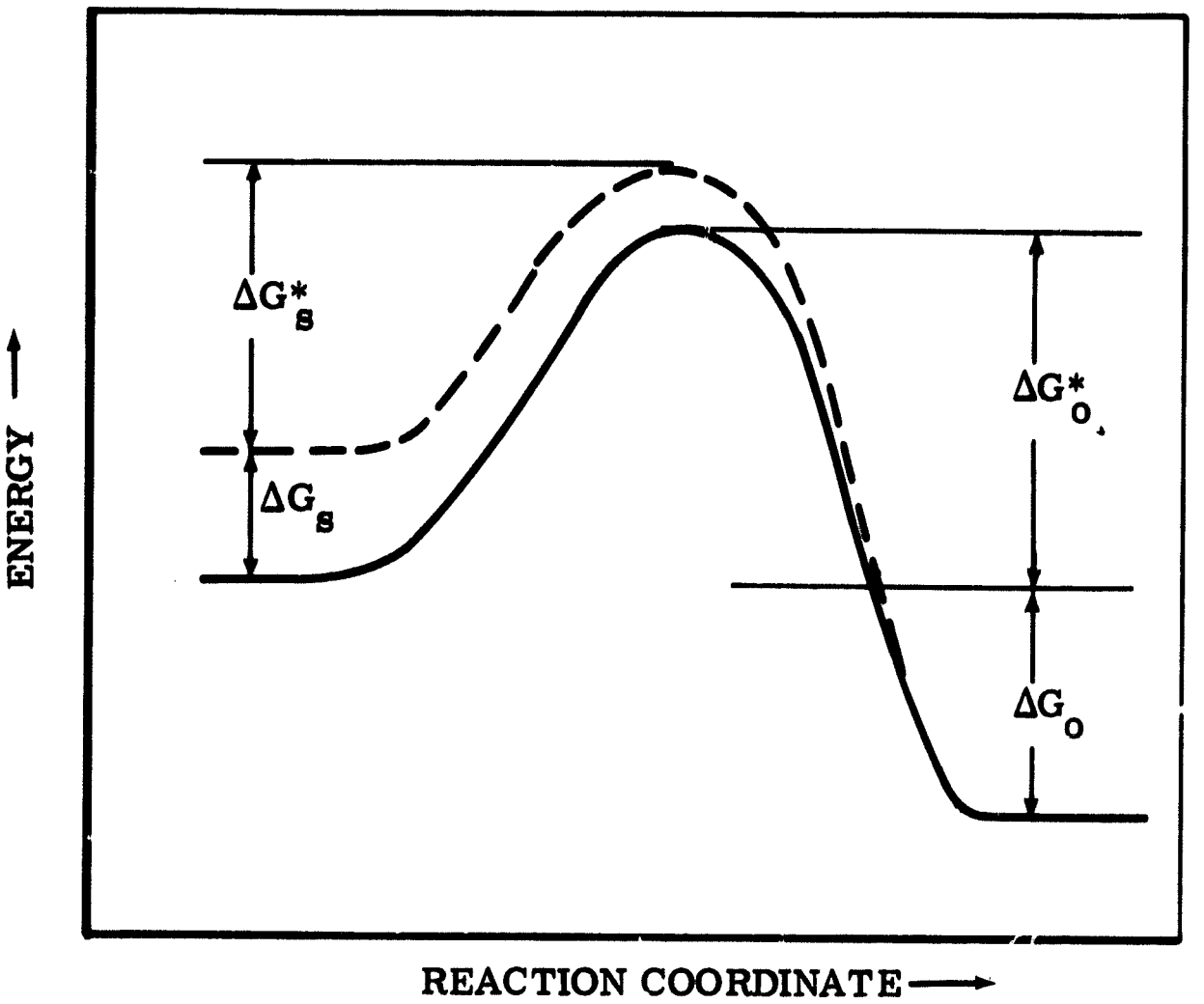

Fig. 41 Generalized energy versus reaction coordinate diagram showing proposed effect of metal atom stress.

$$i = \frac{zF\rho V}{M} \qquad (10)$$

gives a current density of $\sim 3 \times 10^3$ amp/cm^2 for $z = 3$. This current density is not at all unreasonable at a mixed potential at the tip of -800 mv. Current densities of 10^3 amp/cm^2 are not uncommon in electrochemical machining.

We will now consider the implications of the relation of SCC velocity to stress intensity at low stress intensities shown in Figs. 4b and 5 and Figs. 25 through 29 for titanium and aluminum respeccively. The fact that the velocities are less than the mass transport limited value by up to three orders of magnitude indicates that another mechanism is limiting. It is proposed that the velocity is kinetically limited in this region.

There is an interesting similarity between the effect of stress on velocity reported herein for titanium and aluminum and results obtained by Wiederhorn (36) for glass and sapphire. He reports a velocity versus load relationship that is illustrated in Fig. 40. Region I he found to be kinetically controlled, Region II mass transport controlled (water vapor through inert gas in crack) and region III a fast mechanical failure. His terminology for the regions will be used and region I will be reexamined for titanium and aluminum.

A modification of the Hillig and Charles treatment (37) will be used. We will start with the Tafel equation for dissolution at high overpotential, i.e., the mixed potential established at the tip is several hundred millivolts higher than the reversible potential for formation of Ti^{+3}.

$$i = i_o \exp\left(\frac{\alpha n F}{RT}\eta\right) \tag{11}$$

It will be assumed that within the elastic region the free energy of the metal atoms at the crack tip is increased by an amount

$$\Delta G = \frac{\frac{1}{2}M\,\sigma_T^{\,2}}{Y\rho} \tag{12}$$

The effect of this increased energy on reaction kinetics is illustrated by means of Fig. 41. The activation energy at the mixed potential but with no stress is designated as ΔG_o^*. The free energy of the stressed metal atoms is increased by ΔG_s but the free energy of the species in solution side is assumed to be unaffected by the metal stress. It is assumed that the new activation energy

$$\Delta G_s^* = \Delta G_o^* - \alpha_s \Delta G_s \tag{13}$$

where α_s is a transfer coefficient associated with the electrochemical reaction of the stressed metal atoms. The value of α_s will be assumed to be constant, which in effect is to keep the second term in the Taylor expansion used by Hillig and Charles (37) for activation energy and to discard their first term.

Putting the nondimensionalized decrease in activation energy from equations 12 and 13 into equation 11 gives

$$i = i_o \exp\left(\frac{\alpha n F}{RT}\, n + \frac{\frac{1}{2}\alpha_s M \sigma_T}{Y \rho\ RT}\right)^2 \qquad (14)$$

If it is assumed that velocity is linearly related to current density at the tip by equation 10 and that the overpotential is constant for the tip potential determined by a mixed potential (6), then equation 14 can be rewritten

$$V = V_o \exp\left(\frac{\frac{1}{2}\alpha_s M \sigma_T}{Y \rho\ RT}\right)^2 \qquad (15)$$

It is assumed that the surface energy term, $\frac{\Gamma M}{\rho r_T RT}$ of Hillig and Charles (37) is included in V_o because the surface energy, Γ, and the tip radius, r_T, are not yet accessible to independent measurement.

Equation 15 is further modified to test with the experimental data in Region I for titanium and aluminum. The tensile stress, σ_y, in an isotropic elastic medium in the plane of a tensile crack is related to the stress intensity factor and distance from the crack tip by (38)

$$\sigma_y = \frac{K_I}{(2\pi r)^{\frac{1}{2}}} \qquad (16)$$

The tip stress will be assumed to occur at a distance of one atomic radius within the metal phase from the crack tip, or

$$\sigma_T = \frac{K_I}{(2\pi r_a)^{\frac{1}{2}}} \qquad (17)$$

From equations 15 and 17 we get

$$\frac{d \log V}{d K_I} = \frac{\alpha_s M \sigma_T}{2.3 Y \rho RT (2\pi r_a)^{\frac{1}{2}}} \qquad (18)$$

The maximum value that this expression could have would be for the case of ultimate tensile stress at the crack tip, which from Gilman (39) is Y/10. Therefore

$$\left(\frac{d \log V}{dK_I}\right)_{max} = \frac{\alpha_s M}{23 \rho RT (2\pi R_a)^{\frac{1}{2}}} \qquad (19)$$

Assuming $\alpha_s = 0.5$ and $r_a = 2 \times 10^{-8}$ cm gives

$$\left(\frac{dV}{dK_I}\right)_{max} = 2.62 \times 10^{-8} \left[(\text{dyne/cm}^2)\ \text{cm}^{\frac{1}{2}}\right]^{-1}$$

$$\text{or} \qquad 2.9\ (\text{KSI}\sqrt{\text{in}}\ )^{-1}$$

The maximum value of the slope of the log V vs K_I curves for titanium and aluminum in region I is about 1 $(\text{KSI}\sqrt{\text{in}})^{-1}$. The implication of this is that stresses very close to the theoretical limit of these materials is reached at the crack tip. Wiederhorn (36) came to a similar conclusion for his work on glass.

The question remaining to be answered is how stresses approaching the theoretical limit of the material are produced at the crack tip. A model presented earlier (1) is described here again in Fig. 42.

It is proposed as did Kelly, Tyson and Cottrell (40) that the decision as to whether a cleavage crack propagates or whether slip is initiated (thus blunting the crack front) is made on an atomic scale near the crack tip. The modified Griffith treatment of a sharp crack of length in an isotropic, elastic, infinite plate of unit thickness is used. The stress σ_y in the y direction at r distance into the material along the axis of the crack is related to the stress at infinite distance from the crack, σ, by (38)

$$\frac{\sigma_y}{\sigma} = \sqrt{\frac{a}{2r}} \qquad (20)$$

In a real material a plastic zone is formed around the tip of the crack beginning at a distance, r, where the stress, σ_y, equals the yield stress of the material, S_Y. Equation 20 is normalized by S_Y and plotted in Fig. 42. This mode of the theory is already established and is the basis of fracture mechanics.

If it is now assumed that forces for initiation are very large compared to forces for movement of mobile dislocations, then the volume between dislocations or slip bands can be considered as an elastic continuum down to dimensions approaching atomic size. It may be noted that this assumption is implicit in the treatment by Zener (41) of

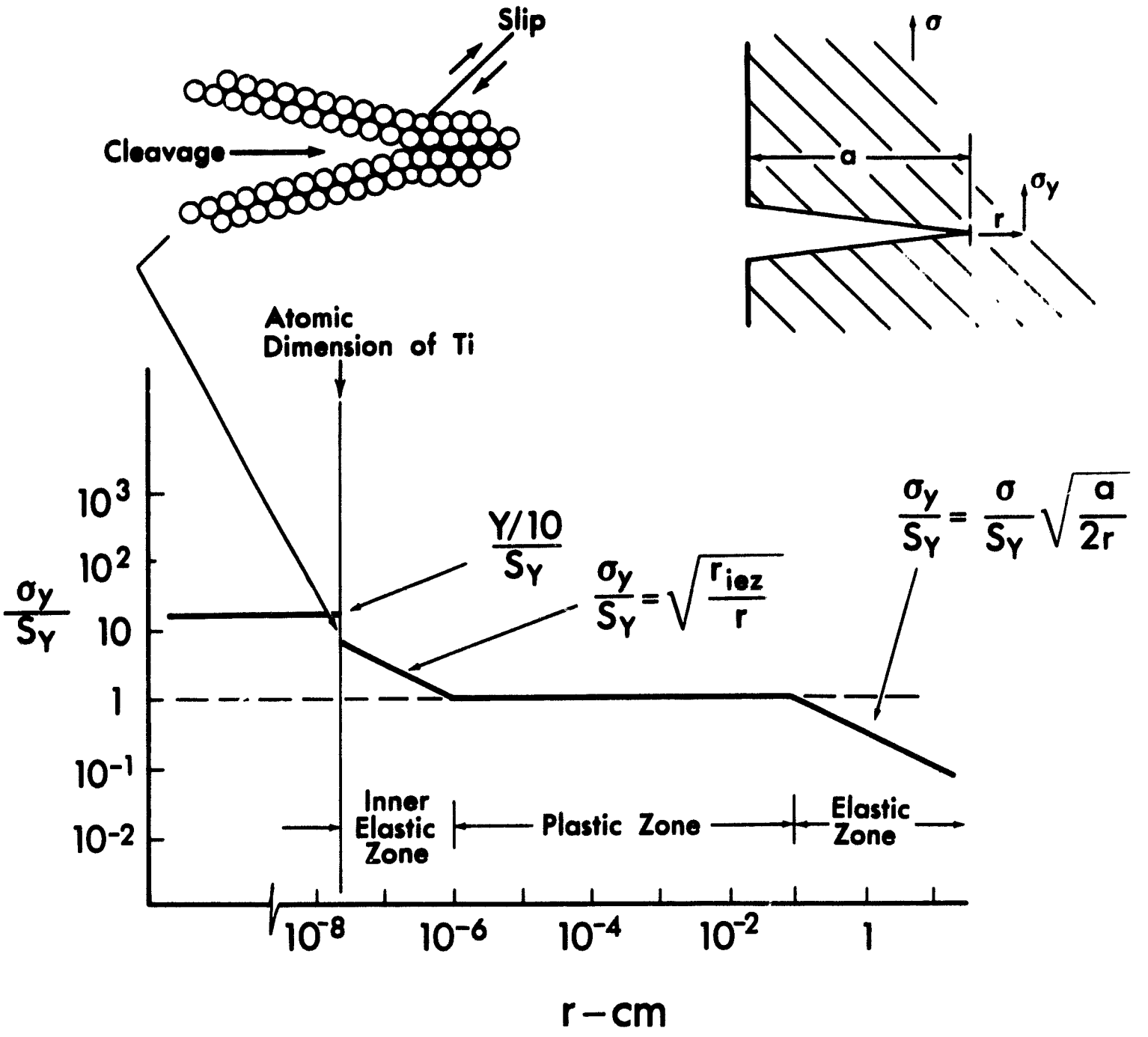

Fig. 42 Proposed model of stress conditions at tip of a crack in a metal.

stresses at grain boundaries caused by dislocation pileups. Assuming the same square root relation for the distance r as in Equation 20 and that $\frac{\sigma_y}{S_Y} = 1$ at $r = r_{iez}$ gives for the "inner elastic zone":

$$\frac{\sigma_y}{S_Y} = \sqrt{\frac{r_{iez}}{r}} \tag{21}$$

An approximation for the distance between dislocations is $r_{iez} = \rho_d^{-\frac{1}{2}}$. Equation 21 is plotted in Fig. 42 for a dislocation density of 10^{-12}cm. This gives about a ten fold increase in stress within atomic dimensions of the tip.

It is proposed that an intercept of Equation 21 at atomic dimensions which equals or exceeds the theoretical strength would cause cleavage to occur without specific environmental effects. The higher intercept could be caused by an increase in yield strength or by a decrease in the mobile dislocation density. This might explain the low strength of the notched mill-annealed specimens in air (6).

The stress conditions for stress corrosion cracking could occur when the intercept of Equation 21 at atomic dimensions is above the yield strength but not quite to the theoretical strength. Ions or species with the right chemical properties could then approach the tip of a crack and selectively attack the stressed metal atoms. Chloride, bromide and iodide ions appear to have this right combination of properties. Fluoride may give too high a corrosion rate and blunt the crack. The oxyanions may react directly with the bare titanium to form oxide and thus cause too

rapid a passivation. Further electrochemical kinetics studies will be made to test these hypotheses.

A further question to answer is why the stress at the crack tip is related to the average stress, σ, if the stress is transmitted through the plastic zone with stress, S_Y. It is suggested that the stress is either transmitted dynamically by viscous forces, possibly aided by work hardening or that the length of the plastic zone is vanishingly small in the plane of the crack.

4.0 CONCLUSIONS

The following conclusions are based on the work accomplished in the period of October 1, 1968 through March 31, 1969.

1. The mechanism of SCC of titanium alloys is independent of crystal structure.
2. All cases of SCC in titanium alloys studied thus far exhibit flat fracture on specific crystal planes exhibiting many features of a cleavage failure.
3. The critical alloy composition for onset of transgranular SCC in Ti-Mn alloys is about 10 weight % manganese compared to 5 weight % aluminum in the Ti-Al system.
4. The fracture path, morphology and velocity are very different for stress corrosion cracking and hydrogen embrittlement in titanium-manganese alloys.
5. Titanium alloys in concentrated HCl solutions and methanol-halide-ion solutions exhibit a stress dependent velocity region (region I) at low stress intensities. The velocities are below the electrochemical mass transport limited velocity (region II).
6. SCC susceptible aluminum alloys show a stress dependent velocity region I and a stress independent velocity region II in neutral aqueous halide ion solutions.
7. Region II SCC velocity varies with potential with aluminum alloys in a manner similar to titanium.

8. Region II SCC velocity in aluminum alloys varies with bulk halide ion concentration consistent with the electrochemical mass-transport-kinetic model developed previously for titanium.
9. Region II SCC velocity for both titanium and aluminum vary with bulk viscosity of glycerol-water solutions of halides consistent with the electrochemical mass-transport-kinetic model.

5.0 FUTURE WORK

The following items of work are planned for the immediate future:

1. Use DCB specimens to study liquid metal embrittlement in order to evaluate similarities and differences with SCC in systems in which environment metal interaction must occur at the crack tip.
2. Focus attention on initiation and propagation processes in very large grained specimens of Ti:10Al, Ti8%Mn, Ti:13V11Cr3Al.
3. Study susceptibility to SCC of Ti:Cu, Ti:AlSi, Ti-V, Ti16%Mn, and Ti-Sn alloys in various solutions.
4. Resolve the problem of chloride analysis of titanium.
5. Extend electrochemical kinetic studies to a wider range of halide concentrations and potentials and to other alloys.
6. Include parallel soluble titanium ion formation in mass-transport-kinetic model.
7. Focus attention conceptually and experimentallly on events at the crack tip.

6.0 REFERENCES

1. Beck, T.R., Boeing Document D1-82-0554, July 1966.
2. Beck, T.R., and Blackburn, M.J., Research Proposal D1-82-0467, August 1965.
3. Beck, T.R., Contract NAS7-489, Quarterly Progress Report No. 1, September 1966.
4. Ibid, No. 2, January 1967.
5. Ibid, No. 3, April 1967.
6. Ibid, No. 4, July 1967.
7. Ibid, No. 5, October 1967.
8. Ibid, No. 6, January 1968.
9. Ibid, No. 7, April 1968.
10. Ibid, No. 8, July 1968.
11. Ibid, No. 9, October 1968.
12. Ibid, No. 10, January 1969 (short letter report).
13. Curtis, G., Boyer, R. and Williams, J.C., to be published in June 1969 Trans. A.S.M..
14. Berger, L.W., Williams, D.N. and Jaffee, R.I., "The Effect of Hydrogen on the Mechanical Properties of Titanium:Aluminum Alloys", Battelle Memorial Institute Rpt. DA-33-019 505-ORD-F (1957).
15. Ripling, E.J. and Mostovoy, S., Materials Research and Standards, 4, 129, 1964.

16. Hyatt, M., to be published.

17. Speidel, M.O., to be published

18. Hyatt, M. and Smith, H., to be published.

19. Mostovoy, S., Crosley, P. B., and Ripling, E.J., Journal of Materials (ASTM) 2, 661, 1967.

20. Sedricks, A.J., to be published in Corrosion.

21. Beck, T.R. and Grens, E.A., J. Electro. Chem. Soc., 116, 177, 1969.

22. Sanderson, G. and Scully, J.C., Conf. on Fundamental Aspects of Stress Corrosion, Ohio State 1967, in press.

23. Williams, D.N., Journal Inst. of Metals (London), 91, 147, (1962-3)

24. Jaffee, R. I. and Williams, D.N., Trans. A.S.M., 51, 820, 1959.

25. Fager, D.

26. Coleman, E.G., Weinstein, D., and Rostocker, W., Acta Met., 5, 491 (1961).

27. Brown, W.E., and Srawley, J.E., ASTM Special Technical Publication No. 410, Philadelphia (1966).

28. VanDerSluys, W. A., University of Illinois, T & AM Report 292, (1966).

29. Srawley, J.E. and Gross, B., NASA Technical Note TN D-3820, (1967).

30. ARPA Coupling Program on Stress Corrosion Cracking, Seventh Quarterly Report, (1968).

31. Novak, S.R., and Rolfe, S.T., Submitted to ASTM for publication.

32. Otsuka, R., Scientific Papers of the Institute of Physical and Chemical Research, 54, 97 (1960).

33. Pourbaix, M., "Atlas of Electrochemical Equilibria", Pergamon Press, New York, 1966.

34. Anderson, J.R., and Gani, M.S.J., J. Phys. Chem. Solids, 23, 1087 (1962).

35. Wilke, C.R. and Chang, P., A.I.Ch.E., Journal, 1, 264 (1955).

36. Wiederhorn, S.M., "The International Journal of Fracture Mechanics", 4, 171 (1968).

37. Hillig, W.B. and Charles, R.J., in "High-Strength Materials", V. F. Zakay, Ed., John Wiley, New York, 1965.

38. Paris, P.C. and Sih, G.C., in "Fracture Toughness Testing and its Applications", ASTM, STP No. 381, Philadelphia, 1965.

39. Gilman, J.J. "Strength of Ceramic Crystals", Am. Cer. Soc. Conf., New York, 1962.

40. Kelly, A., Tyson, W.R., and Cottrell, A.H., Phil. Mag., 15, 567 (1967).

41. Zener, C., Trans. ASM, A40, 3 (1948).

7.0 NOMENCLATURE

a = crack length, in or cm

B = specimen thickness, in

C = concentration, mole/cm^3

D = diffusivity, cm^2/sec

E = Young's modulus, psi

F = Faraday, coul/equiv.

G = free energy, cal/mole

h = beam height, in

i = current density, amp/cm^2

K_I = stress intensity factor

ℓ = distance in crack from apex to position where current and solution flow in from sides, cm

M = molecular weight, gm/mole

n = number of monolayers

n = number of electrons in rate determing step

P = load, lbs

Q_x = charge density of a monolayer, coul/cm^2

R = gas constant

r = distance from crack tip in metal, cm

S_y = yield stress, dyne/cm^2

T = absolute temperature

V = crack tip velocity, cm/sec

V^s = crack tip velocity in pure solvent, cm/sec

$\tilde{V}_A$ = molar volume, cm^3/mole

W = specimen width, in

x = distance, cm

Y = Young's modulus, dyne/cm^2

z = equiv/mole

Greek letters

α = transfer coefficient, dimensionless

Γ = surface energy, erg/cm^2

γ = angle radians

δ = deflection at load line, in

δ^p = distance in crack from apex to end of tip zone, cm

η = overpotential, volts

κ = conductivity, ohm^{-1} cm^{-1}

μ = viscosity, cp

ρ = resistivity, ohm, cm

ρ_d = dislocation density, cm^{-2}

σ = stress, dyne/cm^2

ϕ = potential, volts

ψ = association parameter

Subscripts

A = component A

B = component B

AB = refers to diffusivity of component A in component B

H = hydrogen ion

iez = inner elastic zone

IR = ohmic

0 = standard condition

S = stressed condition

T = tip

$^-$ = anion